



MODERN HELICOPTER AERODYNAMICS

A. T. Conlisk

Department of Mechanical Engineering, The Ohio State University, Columbus,
Ohio 43210-1107

KEY WORDS: rotor aerodynamics, vortex wakes, tip-vortex, computational fluid dynamics,
experiments, dynamic stall, blade-vortex interaction

ABSTRACT

Modern helicopter aerodynamics is challenging because the flow field generated by a helicopter is extremely complicated and difficult to measure, model, and predict; moreover, experiments are expensive and difficult to conduct. In this article we discuss the basic principles of modern helicopter aerodynamics. Many sophisticated experimental and computational techniques have been employed in an effort to predict performance parameters. Of particular interest is the structure of the rotor wake, which is highly three-dimensional and unsteady, and the rotor-blade pressure distribution, which is significantly affected by the strength and position of the wake. We describe the various modern methods of computation and experiment which span the range from vortex techniques to full three-dimensional Navier-Stokes computations, and from classical probe methods to laser velocimetry techniques. Typical results for the structure of the wake and the blade pressure distribution in both hover and forward flight are presented. Despite the complexity of the helicopter flow, significant progress has been made within the last ten years and the future will likely bring marked advances.

1. INTRODUCTION

For over 40 years the helicopter has played an important role in both military and civilian air transportation. In this article we discuss the basic principles of modern helicopter aerodynamics. In the past, the term “helicopter aerodynamics” has been used synonymously with rotor-blade aerodynamics; for the most part, in this article we will consider this to be the case. However, as will

be noted later, the term “helicopter aerodynamics” is now expanding to include interactions between many different helicopter components.

It is worthwhile to note that there are several excellent textbooks in the area including those by Gessow and Myers (1952), McCormick (1967), Bramwell (1976), Johnson (1980), Stepniewski and Keys (1984), and the short monograph by Seddon (1990). In addition, there have been several other reviews which have covered more specific topics. A comparison of predictive capabilities in the 1940s and 1950s with those of the 1980s is given by Gessow (1986). A review of advances in the aerodynamics of rotary wings is given by Johnson (1986). McCroskey (1995) reviews the latest advances in the computation of the rotor wake flow. Caradonna (1992) details the computational techniques employed in the calculation of the helicopter blade and wake flows. Reichert (1985) and Phillippe et al (1985) have reviewed the current state-of-the-art of helicopter design as well as some of the history of helicopter development from a European perspective.

The field of helicopter aerodynamics is a vast one and includes a number of current research problems that are extremely important in their own right. Space limitations preclude an extensive discussion of all of these problem areas. Accordingly, in this review we focus attention for the most part on the nature of the wake of the rotor blades and the loads that the wake induces; we leave aside the issue of turbulence and turbulence modeling in the computation of the rotor wake. In addition, we do not include the issue of the aeroacoustics of the helicopter, which is a critical design consideration and a vast subject area that merits its own review. Performance calculations are considered only as an output of the aerodynamic calculations.

The paper is organized roughly in terms of methodology rather than by performance regime (hover, forward flight, etc) because all of the methodologies discussed here are used throughout the envelope of operation of the helicopter. However, this dichotomy may be somewhat artificial since, for example, experimental results appear throughout the discussion of all of the methods of modeling the rotor wake. In the next section we present an overview of the fundamentals of helicopter aerodynamics.

2. OVERVIEW

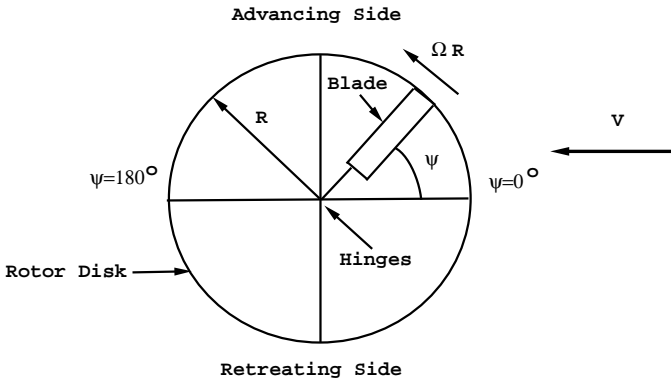
The flow past a helicopter is particularly complicated for several reasons. First, unlike the case of flow over a fixed wing which can often be analyzed by linear aerodynamics, the flow past a rotary wing is never what aerodynamicists consider to be “linear”. This poses significant problems in modeling since numerical simulations need to be iterative in character and experimental observations of highly nonlinear phenomena are often difficult to interpret because of

their complexity. Second, from both an experimental and modeling perspective, it is difficult to study fluid flow in a situation where some components rotate at high speed while other components remain fixed; similar difficulties occur in the area of turbomachinery. For this reason many experiments and modeling efforts have focused on the isolated rotor-blade wake. Only somewhat recently has the effect of the fuselage and tail rotor been incorporated into modeling efforts. Indeed, the helicopter aerodynamicist is faced with the task of analyzing the entire flight envelope of a fixed-wing aircraft from transonic flow to low-speed stall in one rotor revolution. Finally, helicopter experiments are extremely expensive to conduct; this means that significant effort must be put into modeling, which is itself limited by the present state of the art of computing.

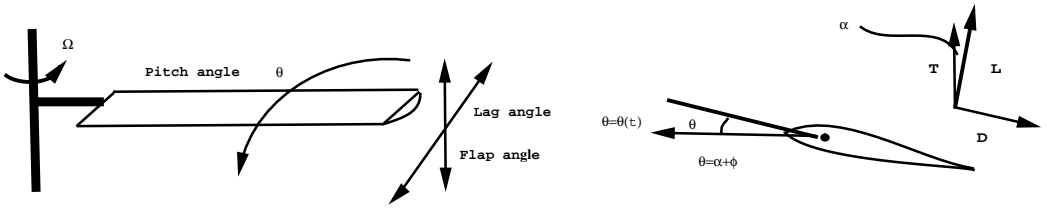
In general, the helicopter is designed to be able to perform tasks that fixed-wing aircraft cannot do, specifically to take off and land vertically (VTOL) and to hover. There are four flight regimes in which the helicopter operates. First, there is hover, in which the thrust generated by the rotor blades just offsets the weight, and the helicopter remains stationary at some point off the ground. The second flight regime is vertical climb, in which additional thrust is required to move the helicopter upward. Third, there is vertical descent, a more complicated flight regime because of the presence of both upward and downward flow in the rotor disk which can induce significant blade vibration. Finally, there is the condition of forward flight, in which the rotor disk is tilted in the flight direction to create a thrust component in that direction. In forward flight, the component of the thrust in the forward flight direction must overcome the drag. Forward flight is characterized by the *advance ratio*, $\mu = \frac{V}{\Omega R}$ where V is the forward flight speed, Ω is the angular speed of the rotor, and R is the rotor radius. Typically, design constraints suggest $\mu \leq 0.4$. Landing is a combination of forward flight and vertical descent.

The main considerations in designing a helicopter are the ability to operate efficiently for long periods of time in hover, high cruising efficiency and speed, range, and payload. All of these considerations are influenced greatly by the aerodynamics of the rotor blades and by other interactions between various components. Unlike fixed-wing aircraft, the helicopter often operates in an unsteady environment; whether in hover or in forward flight, the helicopter operates in, or very near, its own wake which is three-dimensional and highly unsteady. In this review we discuss single-rotor helicopters, although multi-rotor interactions will be discussed briefly in Section 6.

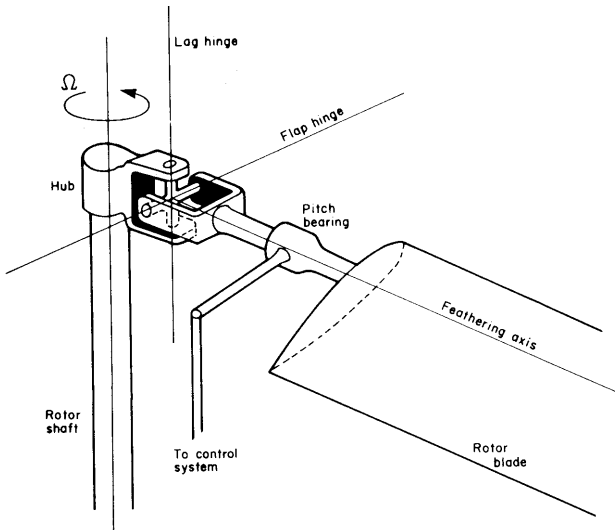
The ideal situation for a helicopter is to achieve a constant lift throughout the rotor cycle. However, since the rotor blades rotate in a single direction, in forward flight there will be a force and moment imbalance. Consider the rotating motion of a single helicopter rotor blade as depicted in Figure 1. As the rotor blade moves in the same direction as the forward flight speed (the



(a)



(b)



(c)

advancing blade side), the velocity near the blade is large and since the lift is proportional to the velocity squared, the angle of attack need not be large to achieve sufficient lift. On the other hand, as the blade moves in a direction opposite to the direction of flight (the retreating blade side) the relative velocity is smaller and the angle of attack must thus be larger to achieve the same total lift. Thus, without a moment-balancing mechanism, the helicopter would tend to roll. To balance the forces and moments, the rotor needs to be *trimmed*; that is, the angle of attack of the blades on the advancing and retreating sides must be adjusted periodically throughout each blade rotation cycle so that there is a balance of moments. This is called *cyclic pitch*. The *collective pitch* of the blades is a control in which the angle of attack (AOA) of each of the blades is increased simultaneously to achieve a higher lift; an increase of the collective pitch, for example, results in climb. In hover, theoretically, trim and flap are not required to balance forces on an isolated rotor; however, non-uniformities and the presence of the fuselage make them necessary. In addition, rotor blades are twisted and often tapered; a twisted blade is one in which the local geometric pitch angle varies along the span.

To provide trim capability and for aeroelastic stress relief, helicopter rotors are often hinged in the sense that the rotor blades must be permitted to bend out of the rotor disk plane as well as pitch to satisfy trim requirements; a sketch of a simple hinging mechanism is also depicted in Figure 1(c). There are two modes in which the rotor is hinged; the *lead-lag* hinge permits motion of the blade within the rotor-disk plane. The *flapping* hinge permits the flapping motion of the blades out of the rotor-disk plane. A rotor having both types of hinges is said to be *fully articulated*. When the blades flap, they no longer trace out a single planar “disk.” In this case we speak of a *tip-path plane* which is the plane whose boundary is defined by the trajectory of the blade tips.

Rotor blades have a large span-to-chord ratio and thus severe stresses can be communicated to the hub if the blades are not permitted to flap. However, if the blades are aeroelastically soft, then hub stresses can be kept to a minimum and both types of hinges can be eliminated. In such cases, the rotor is said to be *hingeless*. Cyclic pitch changes result in changes in the flapping motion. Blade aeroelastic effects play a major role in determining helicopter performance; blade and helicopter aeroelasticity is discussed in Johnson (1980).

The complexity of the flow induced by a helicopter is illustrated by the presence of so many fundamental fluid dynamic research problems. A sketch



Figure 1 A single rotor blade in forward flight. (a) Advancing and retreating sides of the rotor disk. (b) Definition of lift, drag and thrust in hover or vertical climb and lag and flap angles. (c) Sketch of a typical hinge system of a fully articulated rotor; sketch from Johnson (1980).

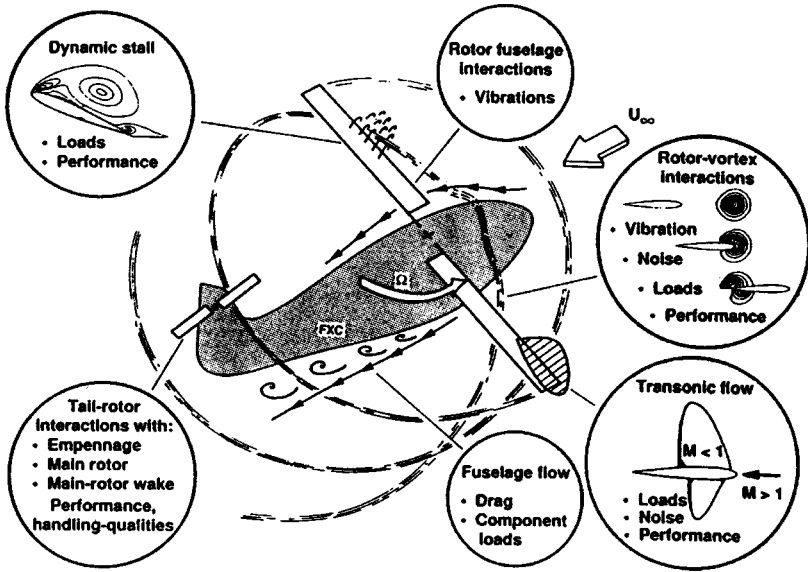


Figure 2 A summary of specific flow problems which occur on a helicopter. From Caradonna (1992).

of the major rotorcraft flow problems is depicted in Figure 2 (Caradonna 1992). First, the flow near the rapidly rotating blade is generally compressible while the flow in the wake of the helicopter rotor blades is likely to be substantially incompressible. Indeed, the flow may be transonic or locally supersonic on the advancing blade side near the tip and thus shock waves will likely be present. On the retreating blade side, because of the trim requirements, the angle of attack is large and the flow may be stalled and so viscous effects are locally important. Moreover, as the blades rotate, the tip vortex shed from one of the blades may collide with a following blade; this phenomenon is known as blade-vortex interaction (BVI) and is a major source of the rotor noise of the helicopter. Blade-vortex interactions are most severe in vertical descent and landing. There will also be interactions between a number of individual components of the helicopter; two important interactions are main-rotor fuselage interaction and main-rotor tail-rotor interaction.

Generally, the wake of a helicopter consists of an inboard vortex sheet and a strong helical tip vortex (Figure 3). The vorticity in the inboard sheet and the tip vortex is confined to very thin regions which are surrounded by substantially irrotational flow. This makes experiments as well as computations extremely difficult because of the rapid variation in velocity near the inboard vortex sheet,

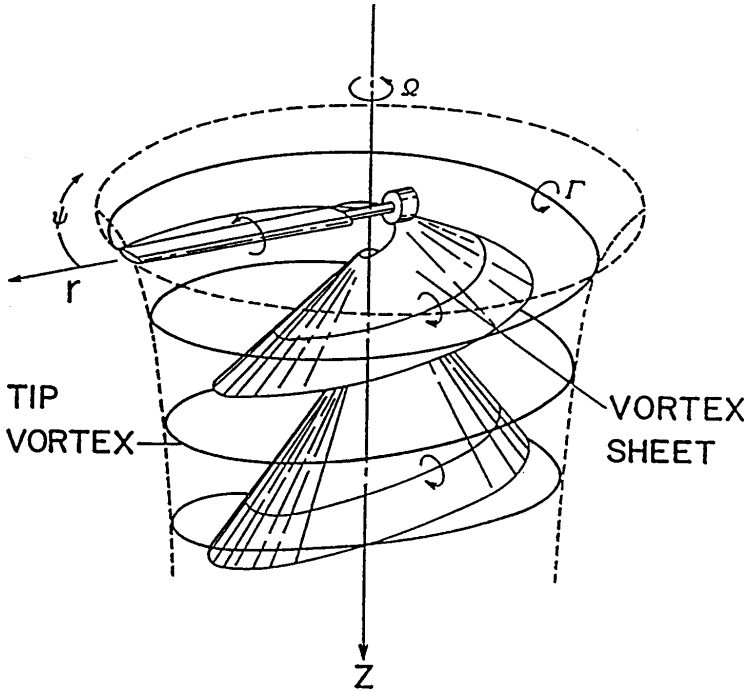


Figure 3 Sketch of a helicopter rotor wake for a single blade. From Gray (1956).

the tip-vortices, and the airframe. Note that the sense of circulation of the inboard sheet is opposite to that of the tip-vortex so that unsteady interaction between the two will occur. There is also a root vortex (not shown in Figure 2) which emanates from the inboard edge of the rotor blade; however, because of the relatively low vorticity near the root, this region is usually not a large factor in design. In addition, there is a wake shed from the rotor hub; hub drag can be a significant portion of the overall drag. However, for brevity we will not discuss the hub flow in this review.

The primary task in rotorcraft aerodynamic design is to determine the lift and drag coefficients of the rotor blades because these two quantities determine the thrust and power required for given speed in forward flight or hover. There are two components to the drag: pressure or form drag, and viscous drag. In situations where loads are generated by three-dimensional vortex systems, the pressure drag is usually called induced drag. Lift is comparatively easy to predict because it is usually found from a surface pressure integration, although this is not the case when the influence of blade-vortex interaction is strong. On

the other hand, the power loss due to drag is very hard to predict because it is a much smaller force and is thus sensitive to small changes in pressure (Ramachandran et al 1989).

From this discussion it is seen that the flow past a helicopter rotor blade features a wide range of velocities from low subsonic speeds to the transonic regime. Moreover, important length scales range from the blade length to the size of the vortex core and thickness of the inboard sheet; these length scales can span several orders of magnitude. Thus modeling and experimentation of helicopter flows are extremely challenging, time-consuming, and costly. Because of these complexities it is difficult to incorporate the dynamic nature of the entire rotor flow in the presence of the helicopter airframe in one single numerical computation or experimental measurement program. For this reason, rotorcraft research tends to be focused on one or two specific aspects of the rotor flow field and tends to have both experimental and computational components. For example, many computational and experimental approaches have focused on the rotor wake flow for the case of two or four rigid blades rotating at relatively low tip-speeds. Under these conditions, it is often not difficult to obtain good results for the blade pressure distribution. On the other hand, at high tip-speeds under forward flight and descent conditions this is often not possible, and a much more fundamental understanding of these flight conditions is required.

3. THE CLASSICAL MOMENTUM APPROACH TO THE ROTOR WAKE

In this section we discuss the foundations of helicopter aeromechanics; first from a purely one-dimensional perspective, and then on the basis of classical thin-airfoil aerodynamics. These powerful methods formed the basis of the design of helicopters up through the 1960s and still provide a basis for assessing the basic trends of helicopter performance today.

Momentum Theory

For both hover and climb (or descent), the analysis of the mechanics of the helicopter began by drawing an analogy with the study of propellers. In the mid-nineteenth century, theories were developed to meet the steady growth of the ship propeller industry. Rankine (1865) developed a simple model of a propeller flow field by applying linear momentum theory derived from the basic relationships of Newtonian mechanics. Subsequently, this early theory was applied to rotorcraft.

During hover, which is the simplest helicopter flight regime, the rotor produces an upward thrust by pushing a column of air downwards through the rotor-disk. If the flow is assumed to be steady, inviscid, and incompressible,

from Bernoulli's equation applied above and below the disk,

$$p_o - p_i = \Delta p = \frac{1}{2} \rho v_\infty^2. \quad (1)$$

In addition, a simple control volume analysis indicates that the thrust generated by the disk is $T = \dot{m} v_\infty$ where $\dot{m} = \rho \pi R^2 v_i$ is the mass flow rate through the rotor-disk. From equation (1), the *induced power* required to drive this process is $P = \frac{1}{2} \dot{m} v_\infty^2$.

The *disk loading* is defined as the thrust divided by the rotor-disk area and from that definition and equation (1), it follows that $v_\infty = 2v_i$, where v_i is the average induced inflow velocity. This indicates that the rotor wake contracts as the fluid velocity approaches v_∞ far from the rotor-disk and the wake radius far from the disk is $r_\infty = \frac{1}{\sqrt{2}} R$; the factor $\frac{1}{\sqrt{2}}$ is called the *contraction ratio* (Figure 3).

A primary parameter by which performance of a helicopter in hover is evaluated is the *figure of merit*. This is defined as the ratio of the power required to produce the thrust (P above) and the total power required $P + P_0$ where P_0 is the *profile power* needed to overcome the aerodynamic drag of the blades and is defined by,

$$FM = \frac{P}{P + P_0}. \quad (2)$$

Typically a well-designed rotor can achieve $FM \sim 0.7 - 0.8$. The difficulty with evaluating the figure of merit is that the induced power is difficult to calculate accurately.

The power required to produce the thrust is crucially dependent on the assumed inflow velocity since $v_\infty = 2v_i$. In early work, the inflow conditions were assumed to be uniform and the influence of swirl in the wake was not considered. The extension of this theory to swirl and forward flight was made later by Betz (1915) and Glauert (1928) respectively.

Despite advances, the prediction of the wake velocity field using momentum theory is not sufficiently accurate because the inflow conditions are difficult to specify accurately, and the effect of detailed blade geometry cannot be considered. The latter issue is addressed by the use of what is called blade element theory and this is considered next.

Blade Element Theory

In blade element theory, the blade is regarded as being composed of aerodynamically independent, chordwise-oriented, narrow strips or elements. Thus, two-dimensional airfoil characteristics can be used to determine the forces and moments experienced by the blade locally at any spanwise location where the local linear velocity is Ωy and y measures distance along the span. The validity

of this assumption was verified experimentally by Lock (1924), who investigated the elements of an airscrew blade. Klemin (1945) determined the induced velocity at the blade as a function of blade radius and Loewy (1957) extended the approach to unsteady flow.

To illustrate the procedure, following Seddon (1990), we write an equation for the differential form of the *thrust coefficient* at a single spanwise location along the blade as

$$dC_T = \frac{dT}{\rho A(\Omega R)^2}, \quad (3)$$

where T is the thrust, ρ is the density, A is the rotor-disk area, Ω is the rotational speed, and R is the rotor radius. The thrust can be expressed in terms of the lift coefficient, C_L , if the angle of attack is small (Figure 1b). In this case, at any blade section where the local velocity is Ωy , $dT = \frac{1}{2}\rho c C_L(\Omega y)^2 dy$ and for N rotor blades

$$dC_T = \frac{1}{2} \frac{Nc}{\pi R} C_L r^2 dr = \frac{1}{2} \sigma C_L r^2 dr, \quad (4)$$

where σ is termed the *rotor solidity* and is the ratio of the total blade area to the total area of the rotor-disk. Here c is the blade chord and $r = \frac{y}{R}$. To obtain the thrust coefficient we integrate along the span and the result is

$$C_T = \frac{1}{2} \sigma \int_0^1 C_L r^2 dr. \quad (5)$$

For small angles of attack, exceptionally simple formulas for C_T can be deduced.

The *power coefficient* is defined in terms of the torque produced in rotating the blades

$$C_Q = \frac{P}{\rho A(\Omega R)^3},$$

and following a similar procedure to that described above, the result is

$$C_Q = \frac{1}{2} \sigma \int_0^1 (\lambda C_L r^2 + C_D r^3) dr, \quad (6)$$

where λ is termed the *inflow factor* and for the case of hover is given by $\lambda = \frac{v_i}{\Omega R}$. Note that in hover, from the definition of the thrust coefficient and the induced velocity, $\lambda = \sqrt{\frac{C_T}{2}}$. The power coefficient, which is the measure of how much power is required to produce lift and to rotate the blades, depends crucially on the drag coefficient.

From this discussion, it is evident that rotor performance depends critically on sectional flow properties; namely, local blade angle of attack and local

Mach number. Consequently, modeling efforts have been designed to predict sectional lift and drag in order to calculate the thrust and power coefficients. However, in blade element theory, the effects of dynamic stall, compressibility, and blade-vortex interactions are usually omitted.

The velocity at the inflow boundary to the rotor crucially depends on the structure of the wake flow. Consider the rotation of the blades started from rest. In the initial stages of the motion, the velocity at the inflow rotor-disk depends on the local flow near the rotor blades. As time passes, the vortex sheet and the tip-vortex shed from the rotor blades begin to extend far below the rotor-disk, forming the rotor wake. At this point, the inflow velocity at the rotor-disk becomes critically dependent on the precise placement of the wake. This is why the calculation of the rotor wake is crucial in calculating the loads on the rotor blades. Vortex methods can predict the unsteady effects of the rotor wake on the blades and on the airframe, and this is discussed next.

4. MODERN THEORETICAL AND COMPUTATIONAL APPROACHES TO THE ROTOR WAKE

The last fifteen or twenty years have seen rapid development of computational and experimental efforts to calculate rotor wake problems. Nevertheless, the accurate and efficient computation of the three-dimensional and unsteady flow around the rotor blades and the rotor wake as a solution of the Navier-Stokes equations remains elusive for reasons that will be explained. In what follows, we outline the basic methods employed in calculating the wake of an isolated rotor.

Gray (1955, 1956) conducted experiments that led to the characterization of the rotor wake as being composed of high-strength tip-vortices and an inboard vortex sheet. This situation is depicted in Figure 3. In modeling the rotor wake by systems of vortices of this type, three approaches have generally been used: rigid wake models, prescribed wake models, and free wake models. In the rigid wake model, the vortex system position is specified as a function of advance ratio and thrust; this situation is compared with results from the experiment in Figure 4. The difficulty with the rigid wake model is that contraction of the wake is not taken into account and thus blade load calculations are in serious disagreement with experiment as rotor solidity, thrust level, and tip Mach number are increased (Landgrebe 1972).

To remedy this weakness, the prescribed wake model (Landgrebe 1972) uses experimental data to locate the wake position and therefore includes wake contraction; this method is discussed in detail in Section 5 where experimental methods are described. This wake method is very efficient computationally. However, experimental data is required and so this method of calculating the

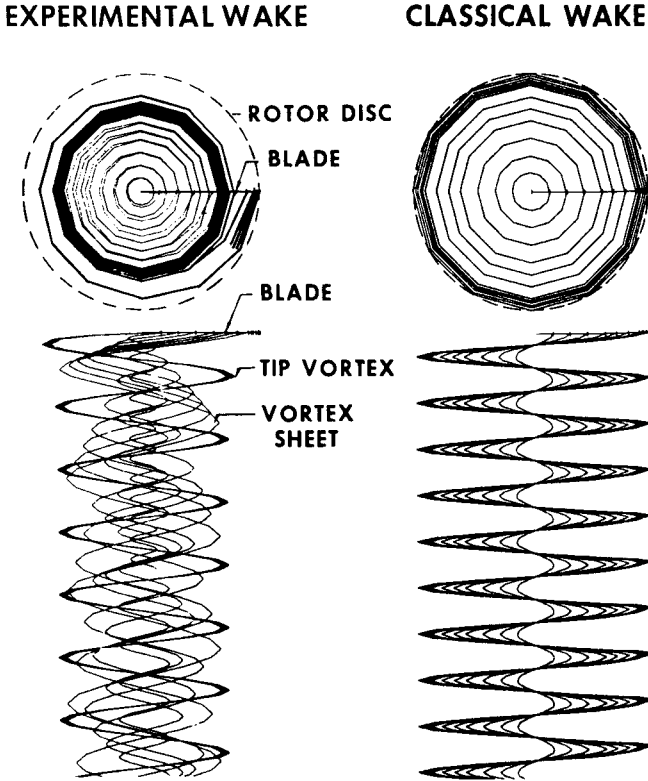


Figure 4 Classical or rigid rotor wake in hover as described by Landgrebe (1972).

wake is not truly predictive. The prescribed wake concept has been extended to numerical prediction of rotor airloads for a range of flight conditions by Egolf and Landgrebe (1983).

In a free wake calculation, the vortex system motion is calculated directly from the effects of all the other wake components and the influence of the blade. In this method, the wake is allowed to develop in time and initial-value, Lagrangian methods are used to determine its position at each time step. This is the industry standard today, and as computers have become faster, the free wake calculation has become more affordable.

There are two means of determining the structure of a given flow field. In a Lagrangian description, individual fluid particles are followed forward in time. In an Eulerian description (not to be confused with the Euler equations), the

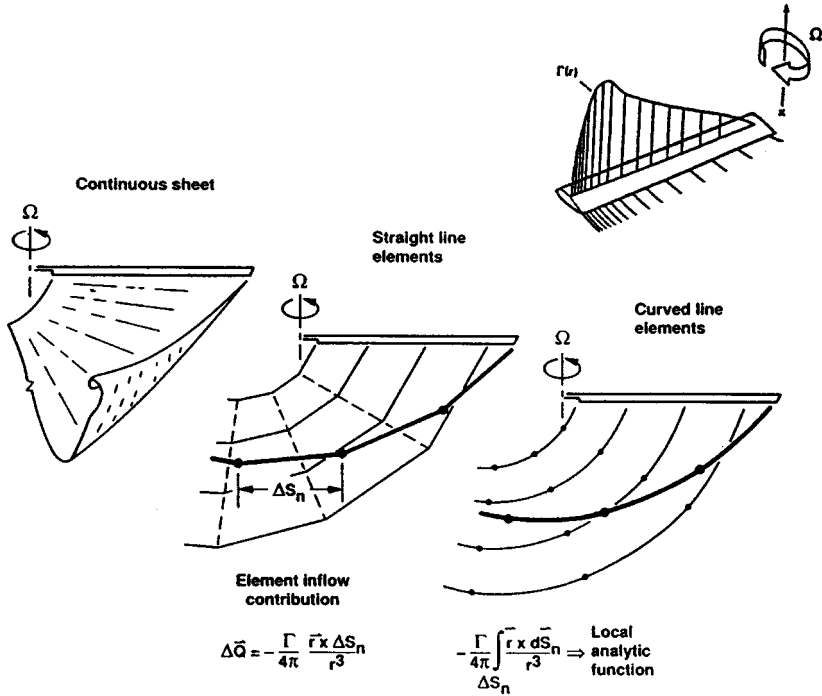


Figure 5 Vortex lattice representation of the rotor wake as described by Caradonna (1992).

solution for the velocity field is calculated at a number of specified field points. Thus an Eulerian description involves a grid system which is not required in a Lagrangian description. In what follows, we consider both sets of methods for calculating the rotor wake.

Langrangian Descriptions of the Rotor Wake

In Lagrangian methods, a specified formula for the velocity field is usually the starting point. In helicopter aerodynamics, these methods correspond to vortex methods; the velocity induced by the vortex itself is usually described by the Biot-Savart law (Batchelor 1967, p. 87) for the velocity field due to an arbitrary patch of fluid containing vorticity. The tip-vortex is usually approximated by a line vortex, and the inboard sheet is often approximated by a vortex lattice; typical representations are depicted in Figure 5.

The Biot-Savart Law is singular when evaluated in the region where the vorticity is nonzero. Thus in order to follow the motion of the wake, some sort

of regularization or smoothing procedure is used. The method is to use a model for the velocity in the core of the vortex to desingularize the Biot-Savart integral; this is termed a cut-off method since the region including and immediately adjacent to the singular portion of the integral is omitted or “cut off” in the calculation. Moore (1972) was able to relate the so-called “cut-off length” to the flow in the vortex core. There are a number of core flows which have been used in rotorcraft applications; the most common is perhaps the simple Rankine vortex in which the core swirl velocity is

$$v' = \begin{cases} \frac{\Gamma}{2\pi} \frac{r}{a_v^2}, & \text{for } r \leq a_v, \\ \frac{\Gamma}{2\pi r}, & \text{for } r \geq a_v. \end{cases} \quad (7)$$

Another distribution was used by Scully (1967) in which the swirl velocity is given by

$$v' = \frac{\Gamma}{2\pi a_v^2} \frac{r}{1+r^2} \quad \text{for } r \leq a_v. \quad (8)$$

In equations (7) and (8) Γ is the circulation, r is the radial coordinate, and a_v is the vortex core radius. Use of these profiles in rotorcraft calculations has recently been discussed by Leishman et al (1995); their results indicate little difference in the profiles when compared with experimental data, although the Rankine profile seems to overpredict the maximum velocity in the vortex when compared with data (Leishman et al 1995).

Scully (1967) used this approach to numerically compute solutions for the rotor wake. Using the swirl velocity given by equation (8), he used the straight line segments of Figure 5 to model the tip-vortex. The inboard vortex sheet was represented by a single large-core vortex located at about midspan. It was found that the tip-vortex is the dominant component of the wake velocity field because its strength is much greater than that of the inboard sheet; this can be seen from the sketch of the bound circulation depicted in Figure 5.

As noted above, the free wake calculation is now the industry standard. This means that the wake is allowed to evolve based on the velocity felt at each point on the tip-vortex and vortex sheet. Once the velocity distribution is determined at each point, the wake must be advanced forward in time using an initial-value problem solver. Typical methods used include first-order Euler, Euler predictor-corrector, and more accurate methods. Because the Biot-Savart Law is only valid for incompressible flow, rotor codes generally employ the Prandtl-Glauert compressibility correction for local sectional aerodynamic loading (Johnson 1980, pp. 262–263).

The advantage of vortex methods is that the wake structure can usually be calculated without numerical dissipation because the size of the vortex core is specified. However, the strength of the wake as measured by the strength of the tip-vortex and the inboard sheet is not known *a priori*. A common way to specify this is to view the rotor blade as a source of lift in which the spanwise concentration of vorticity shed into the wake is concentrated on a single line, usually the quarter-chord of the airfoil. This is called lifting-line theory. This method is simple and adds little computational cost since, for the linearized case, an analytical solution for the circulation is available. The method for a fixed wing in incompressible flow is described in aerodynamics text books (Katz and Plotkin 1991) and the extension to compressible flow for a rotary wing is straightforward (Johnson 1980). For incompressible flow, the amount of bound circulation generated by the lifting line can be calculated by satisfying the Kutta condition (just as for a fixed wing). The result for a small angle of attack at each two-dimensional slice of the blade inboard of the blade tip is

$$\Gamma = \pi c \Omega y \alpha \quad (9)$$

where α is the angle of attack measured from the zero-lift angle of attack. The sectional circulation corresponds to the fixed-wing result with external flow speed $U = \Omega y$ and is depicted in Figure 5; of course, equation (9) is not valid close to the blade tip.

While lifting-line theory is computationally simple and fast, it is well known that it is not valid for large variations in the downwash velocity caused by the vortex wake. To remedy this, some rotor codes use a more accurate lifting-surface method in which the rotor blade is viewed as a wing of zero thickness to calculate the circulation (Johnson 1971). However, if the angle of attack is not small and the blade is near stall, the lift coefficient must often be obtained from experimental data or from a simplified lifting model (Leishman & Beddoes 1989). Airfoil lookup tables are also used to provide the lift and drag coefficients. The static stall angle for many rotor blades is generally in the range of 12–15° although dynamic stall angles may be above 20°.

Egolf (1988) has used a modified lifting-line theory along with a vortex box model to calculate the wake for a forward flight condition. The wake is divided into a number of square “boxes” whose boundaries are vortex filaments of equal circulation. Results for a number of quantities such as local section lift, blade circulation, and BVI-induced blade loading are presented. Bliss et al (1987) describe the implementation of the curved vortex elements of Figure 5 first described by Bliss et al (1983). The motivation of this approach is that curved vortex elements are more natural to describe the wake; they indicate that, using this approach, far fewer vortex segments are required than for the straight-line case.

Most free-wake vortex calculations are subject to time-domain instabilities due to the short-wake instabilities present in any calculation using vortices (Sarpkaya 1989). To counter this, Miller and Bliss (1993) employ a constant-age criterion to establish the steady-state, periodic wake solution which is impossible to obtain in a time-marching scheme. Steady periodic solutions can be obtained at all advance ratios; typically, vortex methods have convergence problems at low advance ratios. On the other hand, the amount of computer time is prohibitive. Subsequently, Crouse and Leishman (1993), using similar ideas, showed that smooth periodic solutions could be obtained with little increase in computation time.

The advantage of the Biot-Savart Law is that it represents in an exact way the velocity field due to a vortex system embedded in a surrounding incompressible potential flow, of arbitrary orientation. However, the computation of an individual vortex system is, on an absolute basis, expensive. For each field point, an integration over the entire area or curve having nonzero circulation is required. If N denotes the number of points on the vortex system to be advanced, then the number of computations required per time step is of the order of N^2 if the number of points used to evaluate the integral is also N ; this is usually, but not always, the case. Thus, methods to reduce the number of calculations required have been investigated. Most if not all of these methods differentiate between a “near” and a “far” field. Given a collocation point on the tip-vortex, let us assume that the near field is that portion of the flow field which is within one vortex core radius of the collocation point. The “far” field is that portion of the flow field which is greater than this; typically, points on different turns of the tip-vortex are “far” from each other and the influence of the induced velocity of one point on the other is relatively small.

This idea has been used by Bliss and Miller (1993) in an attempt to reduce computation time and to increase accuracy in the evaluation of the singular Biot-Savart integral. They employ an analytical and numerical matching technique to calculate the evolution of the rotor wake. The method consists of a “near field” solution for the vortex core flow which is matched to a far field solution (which is effectively a smoothed vortex with a very fat core). The distribution is matched in an overlap region. Results similar to previous work are obtained but at a much lower computational cost when compared to the case of a basic curved-element technique.

An effort to improve on this method has been discussed by Miller (1993). He divides the vortex into a number of “vortex particles” or “vortons”. He found that his basic vortex particle method is significantly faster than both the basic curved element technique and the Bliss and Miller (1993) method. Additional methods to reduce computation time of vortex systems can be found in the review by Sarpkaya (1989).

Torok and Berezin (1993) compare several methods for computing wake-induced airloads. The results are depicted in Figure 6. Figures 6*a,b,c* depict results for a vortex lattice approach using straight line segments (Figure 6*a*), a rigid inner wake and a free tip-vortex (Figure 6*b*), and a curved vortex line approach based on the constant vorticity contour approach (Figure 6*c*), respectively. The constant vorticity contour method (Bliss et al 1987) consists of discretizing the wake with curved vortex elements along lines of constant vorticity. Note the considerable differences in the wake geometry for each of the three methods. The differences are particularly acute near the blade tips where the vorticity field is strongest. For Figures 6*a,b* only the tip-vortex is shown although the entire wake is calculated; for Figure 6*c* the constant vorticity contours along the entire blade are shown. Airload results (not shown) indicate that the constant vorticity contour method compares better with experimental data than the others, especially at low advance ratio, but all the results for the blade loads exhibit significant deviation from experimental data.

Lifting-line and lifting-surface methods for the representation of the body are special cases of a more general class of methods referred to as panel methods. These methods consist of solving for the velocity potential in terms of the fundamental solution of Laplace's equation, which can be a source, vortex, or doublet. The solution is evaluated on the body and the integrals are discretized to lead to a system of linear equations for the unknown elemental strengths which may be solved using standard techniques. Panel methods have been used extensively in helicopter aerodynamics for a number of years. The primary advantage of these methods is that, theoretically, arbitrary body shapes may be considered. Panel methods are usually coupled with a far-wake model or with a grid-based full potential method (see below, in Section 4). The use of panel methods in computational fluid dynamics is reviewed by Hess (1990); applications to rotary wing aerodynamics are discussed by Morino and Gennaretti (1991) and by Caradonna (1992). The method has been used by Maskew (1986) and a new boundary-element formulation of the rotor blade and wake has been described by Gennaretti and Morino (1992).

The methods described so far involve the calculation of the wake-induced airloads in which the wake vortex system is described in terms of the Biot-Savart integral and/or superposition of related elementary singularities. As such, no computational grid in the wake is required, and for this reason the methods described here are normally not viewed as computationally intensive. With the advances in speed and memory of computational hardware, increasingly larger problems may be solved with a finite-difference or finite-volume approach in which the velocities in the wake are calculated directly. These methods are described next.

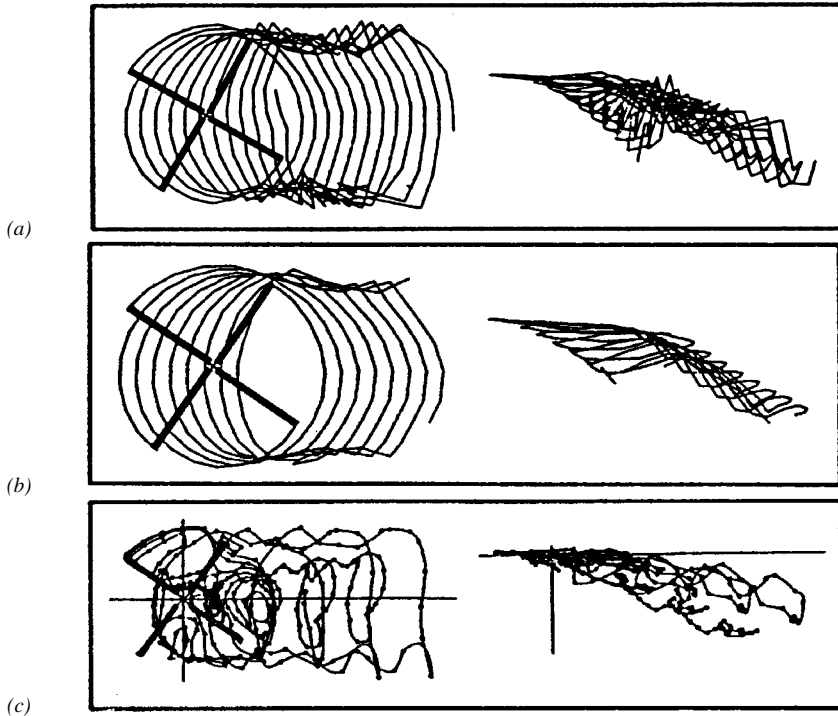


Figure 6 Comparison of various wake models which utilize vortex methods to describe the rotor wake. The tip-vortex only is shown. (a) Vortex lattice, rigid blade; (b) Scully wake, straight line segments; (c) constant vorticity contour method. From Torok and Berezin (1994).

Eulerian Descriptions of the Rotor Wake

In Eulerian descriptions of fluid dynamics problems, the solution for the flow field is computed at discrete points using a specified grid. The term “Eulerian” is distinguished from the “Euler equations” which are the governing equations for inviscid fluid motion. Generally, these methods focus on the near wake of the rotor blade which is often patched to a model for the far wake; the far wake may be a prescribed or free wake.

FULL POTENTIAL METHODS The full potential method is a grid-based method based on velocity potential Φ where $\vec{u} = \nabla\Phi$; compressibility is incorporated directly. The compressible and unsteady continuity equation defines an equation for Φ and using the isentropic relation, $p = K\rho^\gamma$ where K is a reference constant and γ is the ratio of specific heats. Along with Bernoulli’s equation, this defines a system of three equations in three unknowns (p, ρ, Φ) which

can be solved using standard computational techniques. Regions of nonzero vorticity are confined to, at most, vortex sheets and are incorporated by the specification of a jump in potential across the sheet. From Bernoulli's equation, the requirement of a continuous pressure across the vortex sheet yields an equation for the sheet strength according to

$$\frac{\partial \Gamma}{\partial t} + \vec{V}_{ave} \cdot \nabla \Gamma = 0, \quad (10)$$

where \vec{V}_{ave} is an average velocity on the sheet.

Egolf and Sparks (1986) solve the full potential equation using a rotary wing extension of the Jameson and Caughey (1977) fixed-wing code. They couple this solution with a prescribed wake method in which the vortex system is defined using a vortex lattice method. Strawn and Caradonna (1987) use a conservative formulation of the unsteady full potential equation and modify the fixed-wing code of Bridgeman et al (1982). They produce results for a NACA 0012 untwisted, untapered blade and compare the results with those of Egolf and Sparks (1986) and Chang and Tung (1985). Both hover and forward flight results are presented. The circulation convecting from the body is calculated directly from equation (10). Beaumier (1994) discusses the results obtained by coupling a rotor dynamics code with a code which uses straight line vortex segments to model the wake.

Full potential methods, because they are grid-dependent, suffer from the fact that due to inadequate grid size, regions where the vorticity is nonzero diffuse at a much faster rate than that suggested by the influence of viscosity. This affects blade loads and moments, leading to errors in the estimation of various design parameters such as payload capability. To remedy these two deficiencies, a novel approach has been taken by Steinhoff and Ramachandran (1990). The idea is to "embed" the vortex structure into the flow and calculate the effect of the vorticity on the surrounding flow without having to calculate the "vortical" flow itself. The method begins with the decomposition of the velocity field into three parts according to

$$\vec{V} = \vec{\Omega} \times \vec{r} + \nabla \phi + \vec{q}_V, \quad (11)$$

where \vec{q}_V is the velocity field due to the vortical flow. The vortical flow field defined by \vec{q}_V is a model for the vortex sheets and the tip-vortices; it is required to have the properties that it be nonzero inside the region in which the vorticity is nonzero, and zero elsewhere. The vortical flow regions move with the local fluid velocity, and the region of nonzero vorticity is constrained to have a constant thickness, typically of several grid spacings.

Ramachandran et al (1993) solve the full-potential equation on an adaptive grid, and incorporate blade motion. Both cyclic pitch and flapping of the blade

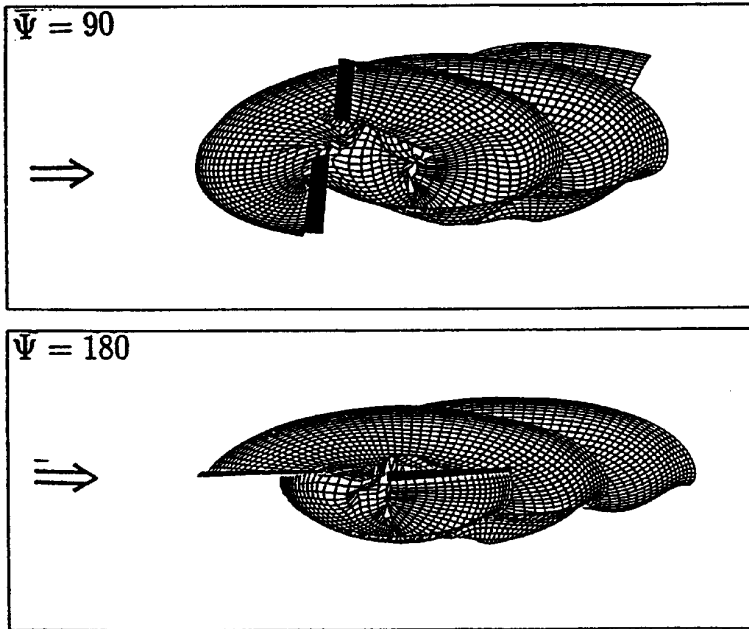


Figure 7 Computed wake geometry at rotor phase angle 90 and 180 for advance ratio $\mu = 0.19$ using the full potential equation with an adaptive grid. No wake model is employed. From Ramachandran et al (1993).

are incorporated and the grid dynamically adjusts to the motion of the blade. Unlike much of the work using a grid-required numerical method, there is no external wake model required. The wake geometry at two rotor azimuths after six revolutions is depicted on Figure 7. The strength of the tip-vortex is seen by the fact that the wake lines bunch near the blade tips; however, the tip-vortex and the inboard sheet do not appear to be distinctly separate as in Figure 1.

NAVIER-STOKES AND EULER METHODS The Navier-Stokes equations are the governing equations of viscous fluid flow and they are the fluid mechanics analogue of Newton's law. Along with conservation of mass, conservation of energy, and an equation of state, three nonlinear equations (six nonlinear partial differential equations) must be solved for the three velocity components, the temperature, pressure, and density. In contrast to vortex and full potential formulations, the Navier-Stokes equations contain the physics for vorticity generation at a surface and subsequent convection into the wake. Moreover, the viscous drag on the blade can also be determined for use in computing

performance variables such as the thrust and power coefficients. Two relatively focused reviews of these methods have been published. Landgrebe (1994) outlines the primary contributions of Navier-Stokes and Euler calculations in the US. A very recent assessment of Euler and Navier-Stokes methods and possibilities of developing new methodologies has been given by Srinivasan and Sankar (1995).

There are several important elements to the calculation of solutions to the Navier-Stokes equations in rotorcraft applications. First, some sort of body-fitted grid generation module is required; this is usually done by some prescribed means, often as the solution to a linear partial differential equation. The generated grids need to be fine in regions where the velocity varies rapidly; these regions include the blade, nose, and tail regions at the tip of the blade and in the viscous boundary layer on the blade. The grid may be structured or unstructured; an unstructured grid is a grid system in which the nodal points are specified in an arbitrary manner. This leaves the wake flow to be covered by a grid system in which the local mesh size is relatively large compared with the thickness of the inboard vortex sheet and the tip-vortex. For this reason, in grid-based computations of the rotor wake, the wake is often smeared out and the location of the wake is sometimes hard to pinpoint. This is in contrast to vortex methods in which the inboard sheet and the tip-vortex structure are specified to a large extent.

Second, to discretize the convective terms in the Navier-Stokes equations, some form of upwinding is required; typically third-order upwinding is used although fifth-order upwinding is now becoming popular in an effort to preserve accuracy (Bangalore and Sankar 1996). Finally, some time-advancing scheme is required and this can be either explicit or implicit. Typically, modern rotor codes employ a first- or second-order implicit time advance algorithm. There is generally an option to calculate solutions to the Euler equations rather than Navier-Stokes; in general, the Navier-Stokes solutions compare better with experiment. While not explicitly discussed in this review, rotor codes include a turbulence model; different turbulence models can lead to different results (Srinivasan et al 1995).

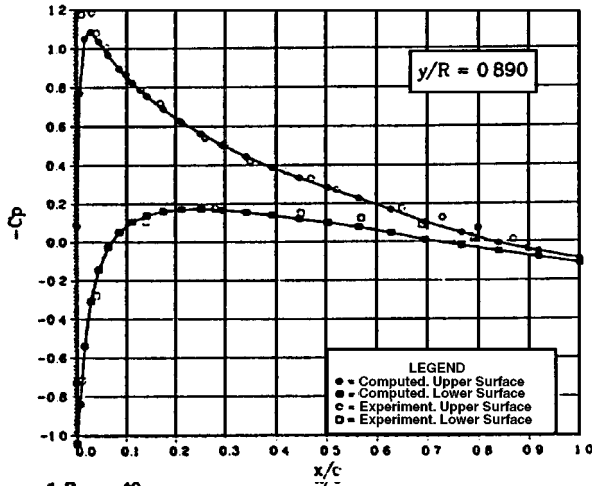
The Navier-Stokes equations for an isolated rotor in hover are usually solved as an initial-value problem with the rotor started from a given state; the equations need to be integrated to steady state. This is very difficult, especially in hover and low-speed forward flight, because of the number of grid points required to resolve the flow for a relatively large number of time steps. Typically, more than two turns of the rotor are required to establish steady state, and by this time, due to numerical diffusion, the strength of the tip-vortex and the inboard sheet are much weaker than those seen in experiments. This is especially true at the high disk loadings required in helicopters today.

Complicating the computation is the need to trim the rotor. Many of the Navier-Stokes computations described here are, at most, only partially trimmed using an external comprehensive rotor design code. At the present time, computational time limitations prevent adding a trim module to the codes. Cyclic and collective pitch settings are calculated from the comprehensive rotor code and then input to the CFD rotor blade code and the flow field is computed. The thrust and power coefficients may then be calculated and the values reinserted into the rotor design code in which the rotor is trimmed again. This process may be continued until the rotor and trim solutions are compatible.

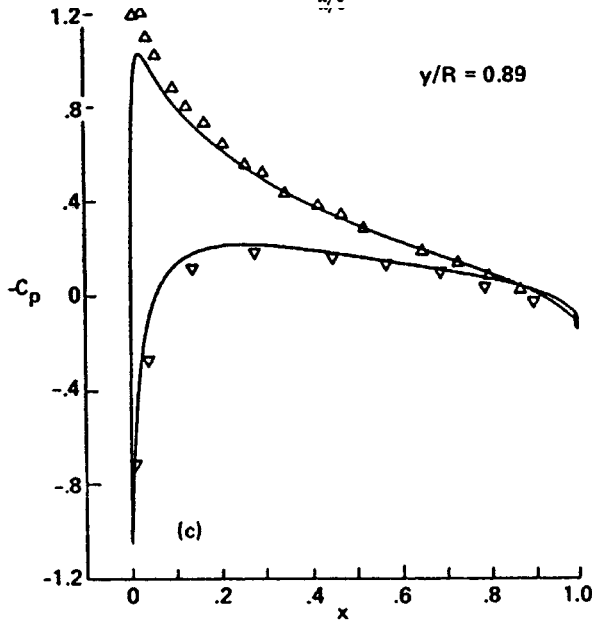
Wake and Sankar (1989), in a paper first presented at the American Helicopter Society National Specialists' meeting on Aerodynamics and Aeroacoustics in 1987, were the first to present solutions to the unsteady Navier-Stokes equations for a rigid rotor blade. They solve the compressible three-dimensional Navier-Stokes equations and compare their computational results with the experimental data of Caradonna and Tung (1981) in the nonlifting, transonic regime for an ONERA blade; results are also produced for a lifting, NACA-0012 blade. A C-grid is used to describe the domain near the blade. The numerical procedure to solve the equations is a fully implicit procedure in space, and is based on a Beam and Warming scheme (Beam and Warming 1978). The far-wake field is either extrapolated from the interior of the computational domain or set equal to zero. Rotor inflow conditions are specified by the transpiration velocity technique which requires the effective angle of attack of the wake; this parameter is fixed externally using a rotor design code. The computational results for the blade pressure in hover are depicted in Figure 8*a*. Forward flight results are also presented, and the comparisons with the experimental results for rotor phase angles in which the flow remains subsonic are good; at higher free-stream Mach numbers where the flow may be locally supersonic over a good portion of the blade, the agreement is not as good.

Srinivasan and McCroskey (1988*a*) solve the unsteady thin-layer Navier-Stokes equations for the same conditions as Wake and Sankar (1989). The thin-layer Navier-Stokes equations are a subset of the Navier-Stokes equations in which the streamwise and blade-spanwise derivatives are neglected in the viscous terms. A typical result for the pressure distribution is depicted in Figure 8*b*; these results are very similar to those of Wake and Sankar (1989) thus indicating that, at least for the blade pressure distribution, solutions for thin-layer Navier-Stokes equations do not differ significantly from solutions for the full Navier-Stokes equations.

As mentioned earlier, all current Navier-Stokes calculations of the rotor wake suffer from numerical diffusion in the sense that the vortex system is considerably smeared. Thus, the fact that the blade pressure distributions depicted in Figure 8 seem to agree well with experiment is somewhat surprising. However,



(a)



(b)

Figure 8 Surface pressure distribution for a lifting rotor in hover. $M_{tip} = 0.44$, collective pitch 8° , $Re = 10^6$ for the experimental data of Caradonna and Tung (1981). (a) From Wake and Sankar (1989) using Navier-Stokes. (b) From Srinivasan and McCroskey (1988) for thin-layer Navier-Stokes; the solid line is the computation.

note that there are significant relative errors in the pressure especially near the tip and at the root. Moreover, it must be pointed out that the results of Figure 8 depict pressures at only one section of the rotor blade; these local section errors often lead to large errors in the integrated lift and normal force coefficients and pitching moments. Industry design requirements suggest that it is necessary for computations to agree with experiments to about 1% for blade loads. Significant improvements to the computational scheme described by Srinivasan and McCroskey (1988*a*) were made and reported by Srinivasan et al (1992). Wake and Egolf (1990) have formulated the problem for use on a massively parallel (SIMD) machine using thousands of processors. Massively parallel architecture is a means for making these computations more affordable.

The influence of the far-field boundary conditions used in a given Navier-Stokes computation have been discussed by Srinivasan et al (1993). The usual boundary condition for an isolated rotor in hover is to assume that outside a suitable computational cylinder, the velocity vanishes. This means that the fluid merely recirculates within the computational box; clearly, this seems unphysical in the sense that the rotor continuously draws fluid into the rotor-disk from outside the box. To remedy this inconsistency, Srinivasan et al (1993) model this process with a three-dimensional sink to satisfy mass flow requirements. A sketch of this boundary condition is depicted in Figure 9*a*; the influence of this new boundary condition is depicted in Figure 9*b* where the sectional thrust distribution is depicted. Note that the results for the new boundary condition are in better agreement with experiment especially near the blade tip where errors are normally larger.

Solutions for the forward flight regime have also been produced. For this condition, blade-vortex interaction may occur and, even in the absence of significant blade-vortex interaction, forward flight computations are much more difficult than hover. Srinivasan and Baeder (1993) have produced solutions for a forward flight condition of $\mu = 0.2$ and a blade tip Mach number of $M_{tip} = 0.8$. In this case, the flow is locally supersonic near the nose of the blade and so a shock forms. The presence of the shock is indicated by the very large surface pressure gradient on the upper surface of the blade as shown in Figure 10. Both Euler and Navier-Stokes solutions are computed using the Baldwin-Lomax turbulence model; the agreement with experiment is similar to that of Figure 8. The good agreement with the Euler solution just aft of the shock is probably fortuitous.

Ahmad and Duque (1996) include moving embedded grids in their calculation of the solution for the rotor system of the AH-1G helicopter. The embedded grid procedure allows a more efficient and more accurate calculation of the flow near the blade under both pitching and flapping conditions; the rotor is partially trimmed externally. The time-accurate calculation is started from freestream

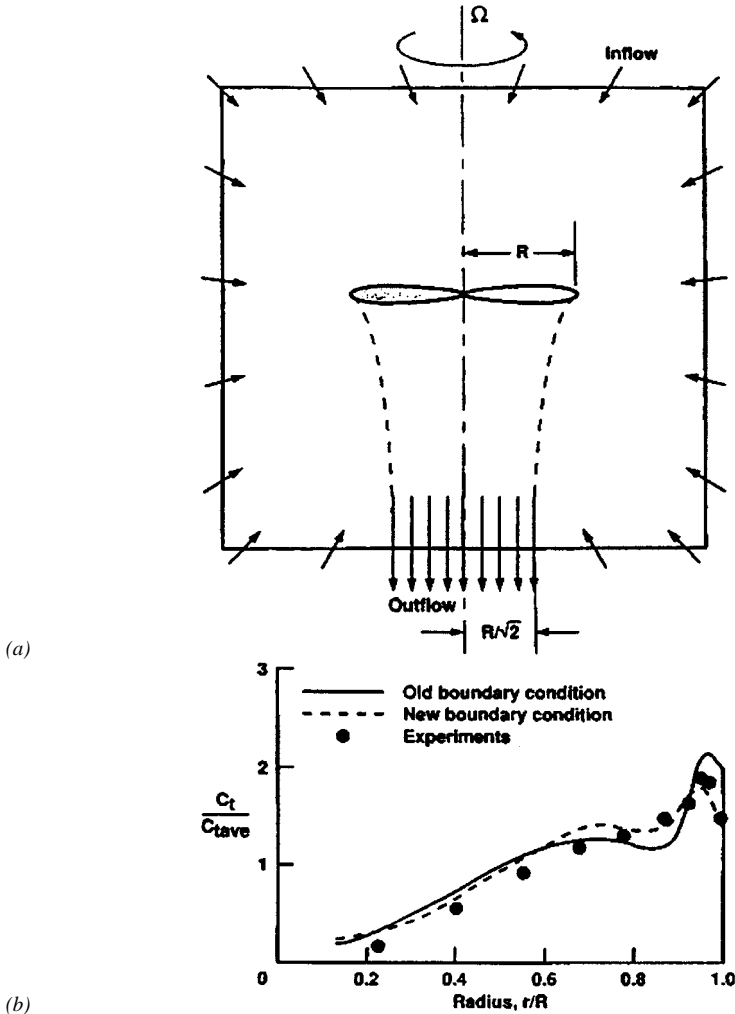


Figure 9 Effect of far field boundary conditions on the rotor wake calculation for a single rotor. (a) Schematic of the new set of boundary conditions. (b) Sectional thrust distributions for the UH-60 rotor; here $M_{tip} = 0.63$, $\theta_c = 9^\circ$, $Re = 2.75 \times 10^6$. From Srinivasan et al (1993).

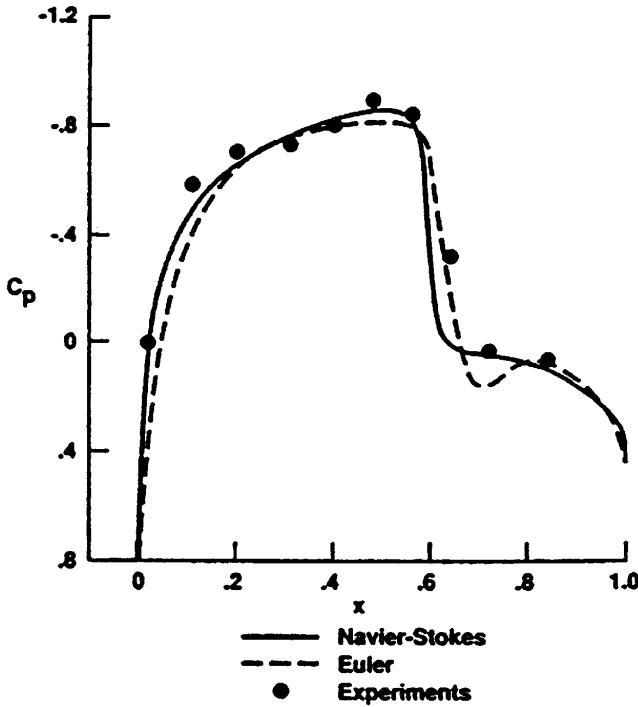


Figure 10 Instantaneous surface pressure distribution at $\psi = 120^\circ$ for a nonlifting rotor in forward flight. Here $M_{tip} = 0.8$, $\mu = 0.2$, $Re = 2.89 \times 10^6$, at $y/R = 0.89$. From Srinivasan and Baeder (1993).

conditions and five complete rotor revolutions are calculated. A typical result for the rotor wake is shown in Figure 11. The wake streaklines exhibit periodicity in about two rotor revolutions; note that while the streakline patterns clearly show the trajectory of the tip-vortex, the magnitude of the vorticity in the tip-vortex may be very small, indicating significant diffusion. The blade pressure and section normal force show significant differences when compared to experiment and the power is overpredicted by 15%. These comparisons are typical of forward flight computations. The complete unsteady calculation takes a total of 45 hours of single-processor CPU time on a Cray C-90 supercomputer and generates 40 Gb of flowfield data.

The results discussed above for the Navier-Stokes equations include a time-stepping algorithm; as such computational error grows with time and in general, solution accuracy degrades substantially after only about one turn of the rotor. Since numerical diffusion increases with time, the accuracy of blade loads is substantially degraded and this is exacerbated at full scale by the aeroelastic

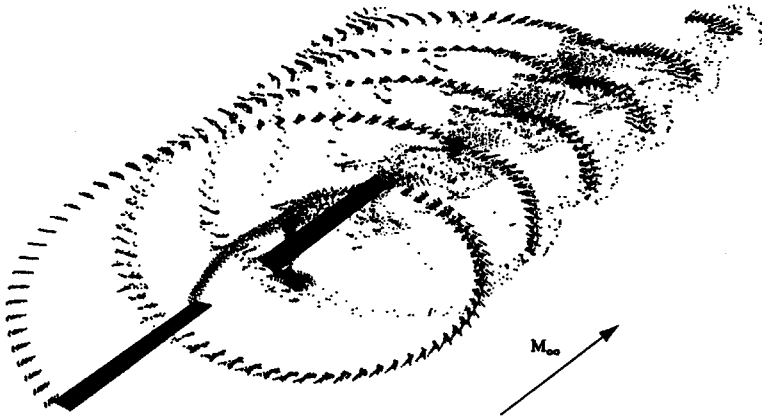


Figure 11 Streaklines for a rotor wake at $\mu = 0.19$. Flow periodicity is established in about two rotor revolutions. From Ahmad and Duque (1996).

deformations and flapping motions. On Figure 12 are results from Bangalore and Sankar (1996) for a UH-60A rotor for two values of rotor phase angle. Note the significant discrepancy between the computations and experiment on the retreating side while the early time results are fairly accurate.

An unstructured grid has great advantages in locally adapting the grid in these regions by allowing insertion and deletion of grid points. Strawn (1991) has applied the unstructured adaptive grid methodology to a rotor wake prediction. In a subsequent paper, Strawn and Barth (1993) use about 1.4 million tetrahedral elements in their solution to the unsteady Euler equations for a hovering rotor model. Even with this fine unstructured grid, the numerical diffusion becomes so large that the calculated tip-vortex core size is considerably larger than observed in the experiments. Additional improvements in the generation of the grid which involve the coupling of overset structured grids with solution-adaptive unstructured grids have been reported by Duque et al (1995).

A method designed to counteract the excessive diffusion of vorticity in the wake is described in a review by Steinhoff (1994). The basic method is similar in concept to the vortex-embedding method and entails inserting an additional term in the Navier-Stokes equations which acts as an external force to prevent diffusion of vorticity. Vorticity diffusion may be illustrated by reference to the Lamb vortex; for this two-dimensional vortex with a viscous core, the nominal radius of the vortex core increases with time as $a_v \sim \sqrt{\nu(t + t_c)}$ where ν is the kinematic viscosity and is small and t_c is the radius of the vortex at its creation. For air, the kinematic viscosity is $\sim 2 \times 10^{-6} \frac{m^2}{sec}$ and so the vortex

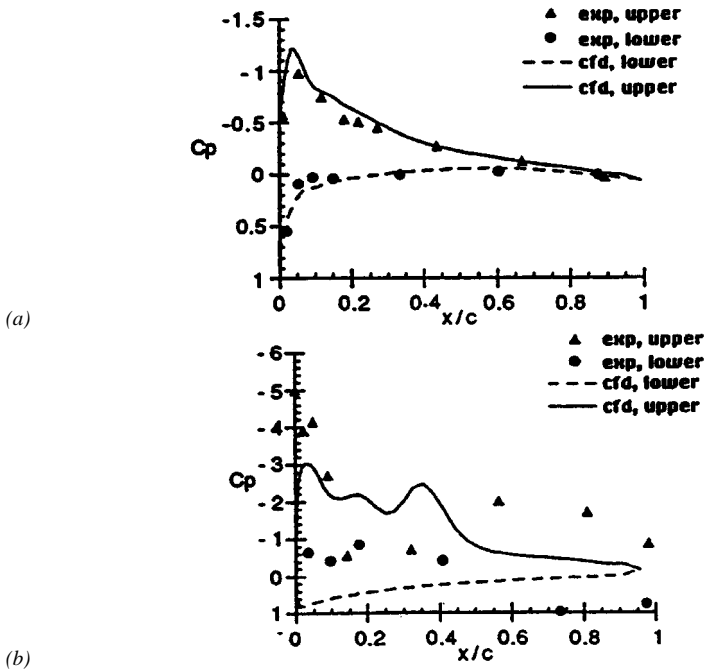
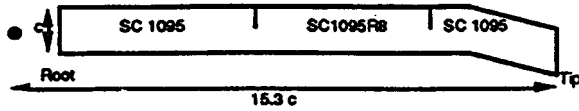


Figure 12 Surface pressure coefficient for $M_{tip} = 0.628$, $\mu = 0.3$, for the UH-60A baseline rotor at (a) $y/R = 0.775$, $\psi = 30^\circ$; (b) on the retreating side at $y/R = 0.4$, $\psi = 320^\circ$. From Bangalore and Sankar (1996).

would be expected to increase substantially in radius only on a very long time scale. This means that in any computation having a time scale much shorter than this viscous time scale, the vorticity within the vortex should not diffuse. A similar comment applies to the inboard vortex sheet.

Steinhoff (1994) forces this to be the case by inserting an external force in the Navier-Stokes equations acting in a direction normal to the vortex sheet and one such choice is

$$\vec{F}_E = -\epsilon \hat{n} \times \vec{\omega}, \tag{12}$$

where ϵ is a parameter which controls the size of the convecting regions of

significant vorticity (i.e. the inboard vortex sheet and the tip-vortex), and \hat{n} is a unit vector in the direction of the normal to the boundary of the non-zero vorticity region. With relevance to helicopter aerodynamics, the method has been applied to incompressible blade-vortex interactions (Steinhoff and Raviprakash 1995) and shows promise for compressible wake calculations.

Performance parameters can be calculated directly from the CFD calculations discussed in this section. Tung and Lee (1994) have compared performance parameters such as the figure of merit and the section thrust and torque coefficients for several different methods of calculating the rotor wake of an isolated rotor in hover. Generally the agreement is adequate with the model-scale data set, although significant differences of up to 10–20% near the blade tip are observed. Moreover, moments due to drag effects are more difficult to predict: Little or no experimental data for drag is available for comparison with the computed results.

The rotor wake is complicated by two additional physical problems which are exacerbated by the pitching and torsional motion of the rotor blades: These are blade-vortex interactions and dynamic stall. These are significant issues in their own right and the problem of dynamic stall has been discussed in reviews of the problem on fixed-wing aircraft. Here we discuss the problems briefly within a rotorcraft perspective.

Blade-Vortex Interactions

One of the most difficult problems with helicopter operation is the occurrence of rotor-blade tip-vortex interaction. Blade-vortex interaction (BVI) is defined as the interaction between a tip-vortex shed from a given blade and another following blade and is most severe when the vortex approaches the blade approximately aligned with the spanwise axis of the blade. This means that the interaction between the vortex and the rotor blade is nearly two-dimensional. A sketch of a direct collision is depicted in Figure 13 from McCroskey (1995). As the blade rotates, pitches, and flaps, the origin of the tip-vortex at the blade tip varies in position; thus, combined with its self-induced motion, the shed tip-vortex may pass very near or collide with a following blade. Blade-vortex interaction is rare in hover, can occur in forward flight, but may be particularly severe during maneuvers, in vertical descent, and in landing (forward flight descent). There is a large body of work in the literature on various aspects of BVI and the noise produced as a result. Due to space limitations we discuss only briefly the main characteristics of BVI. Reducing the number and intensity of blade-vortex interactions is critical for reducing rotor noise.

BVI noise is one of the two major components of impulsive noise associated with the flow past the rotor blades, the other being high-speed impulsive noise due to the high tip Mach number on the advancing side of the rotor (McCroskey

1995, Gallman et al 1995, Heller et al 1994, Gorton et al 1995a). BVI can occur on both the advancing and retreating blade sides, but from an acoustic point of view, the interactions on the advancing side are more important because of the higher Mach number there. As pointed out in the review by McCroskey (1995) and which can be verified by a simple dimensional analysis, the most important parameters in the blade-vortex encounter are the strength of the vortex and its distance from the blade. Prediction of the magnitude of the acoustic signal in the far acoustic field is limited by the accuracy of the calculation of the location and strength of the tip-vortex; small changes in miss distance can result in significant differences in the nature of the acoustic field. From this short discussion, it is evident that a highly accurate computation of the local blade loads during BVI is necessary for an accurate calculation of the noise field.

Generally, for a two-bladed rotor, BVI can commence late in the first quadrant of the blade motion ($\psi \sim 60^\circ$) and is completed near $\psi \sim 180^\circ$. The precise extent of the influence of BVI depends on a number of factors including forward flight speed and tip Mach number. Computational models have been developed for the prediction of the loads during BVI; a few of the many papers include Caradonna et al (1988), Srinivasan and McCroskey (1988b), and Srinivasan and Baeder (1992). In these papers, the vortex structure is specified and fixed

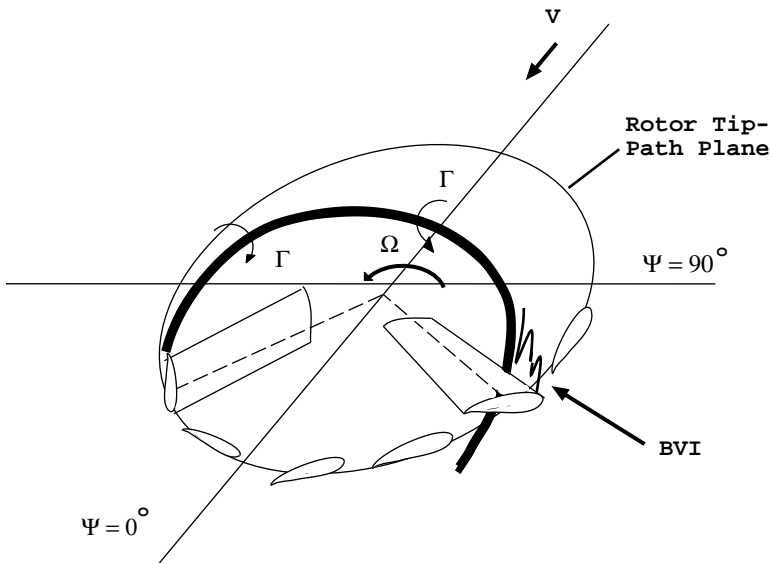


Figure 13 A sketch of a direct collision between a blade and a vortex. From McCroskey (1995).

in time, and the position of the vortex, and hence the blade loads, can therefore be calculated fairly accurately. For example, Caradonna et al (1988) solve the three-dimensional full potential equations; good agreement with experimental data was obtained for both parallel and oblique vortex interactions when the core size of the vortex is fixed in time. However, when the structure of the vortex is calculated along with the balance of the solution of the rotor wake, the results are not nearly as good. Moreover, a number of blade-vortex interactions are expected to occur over a single blade cycle.

Lorber (1991) has experimentally investigated BVI in the forward flight-descent regime for a four-bladed rotor. He was able to map regions where BVI is expected; both retreating and advancing BVI events were found. He was also able to develop a model using a simple wake distortion model and the agreement with experiment is encouraging although some BVI events in the experiments were not predicted in the computations. See also Gorton et al (1995a) for additional experimental results.

A detailed study of multiple self-generated BVI encounters has been given by Hassan et al (1992). They solve the Euler equations to produce results for a number of BVI encounters during a single rotor revolution. The solutions are found to be extremely sensitive to the value of the vortex core radius chosen. A typical result at two inboard stations is depicted in Figure 14. In these results, BVI commences at around $\psi \sim 60^\circ$. Note that agreement with the experimental values is good until about $\psi = 90^\circ$; note the differences between vortices of different core radius. These results are typical of results at other inboard stations as well and reflect the fact that the surface pressure is extremely sensitive to the position and structure of the vortex system relative to each blade.

The strength of the tip-vortex as measured by its circulation is a strong function of the blade tip shape from which it was shed. Consequently, much research has been done to determine if BVI noise can be reduced by suitable design of the tip shape (Yu 1995).

Dynamic Stall

The flow field on the retreating blade side of the rotor is much different from the flow on the advancing side since the rotor must be trimmed. Because of the need for higher lift on the retreating blade side due to the lower relative velocity, the effective blade angle can become relatively large and dynamic stall can occur. The term dynamic stall refers to the process by which a separation bubble forms on the body, grows in size and eventually leaves the body as it is shed downstream. This process induces an additional lift which can be useful but is eventually lost as the stall vortex leaves the surface. At the same time, a dramatic increase in drag and moment also occurs. This large increase in

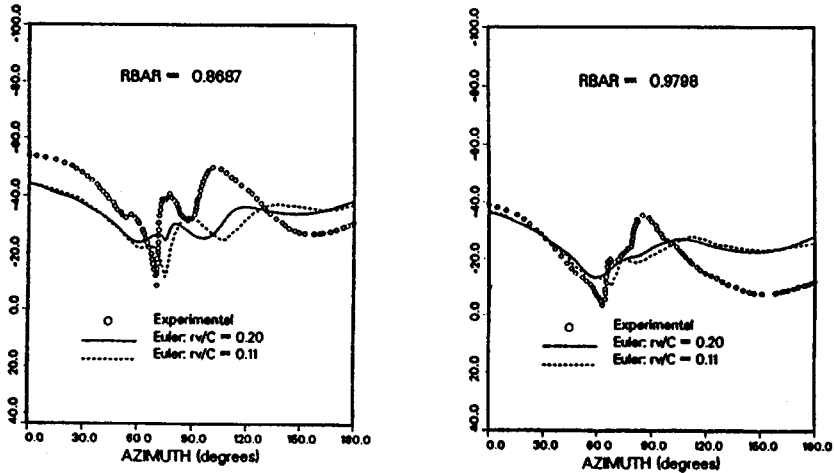


Figure 14 A comparison of predicted and measured surface pressures for the model OLS rotor under BVI conditions at two different inboard locations; three BVI interactions occur during this time range. Here $RBAR = \frac{v}{R}$ and $\frac{rv}{C}$ is a dimensionless vortex core radius. The tip Mach number $M = 0.67$, advance ratio 0.1632. The distributions are at 3% chord. From Hassan, Tung and Sankar (1990).

moment induces significant vibratory loads. There have been a large number of studies of dynamic stall on wings and there have been several reviews on the subject including Carr (1988) and McCroskey (1981). Consequently, in deference to existing recent reviews, we limit our discussion of this topic here.

It has long been recognized that the flow past the rotor blade is at least locally two-dimensional at a given blade section. Two-dimensional dynamic stall calculations for rotorcraft have been common over the years (Ham and Garelick 1968). Consequently, much of the current work on dynamic stall is in the two-dimensional arena (Carr and Chandrasekhara 1995).

From a rotorcraft perspective, the stall vortex is an additional source of vibration of the rotor blade complicating the calculation of the generation and evolution of the rotor wake. Substantial additions to the data base on finite wings oscillating in subsonic flow are the experiments of Lorber et al (1994). They studied three-dimensional dynamic stall on several rotor blades in order to determine geometric effects on performance and stall boundaries in both steady forward flight and descent conditions. They measured blade pressures and identified a regime where stall occurs followed by the detachment of the stall vortex identified as an aft propagation of its suction peak. Laminar and turbulent flow regimes are identified as well. Srinivasan et al (1995) discuss

the influence of turbulence models and numerical dissipation on the modelling of the stall process.

The investigations of the means of controlling the dynamic stall process are just now beginning; Yu et al (1995) discuss the influence of the presence of a leading edge slat, the effect of deformable airfoils, and the effect of blowing on the formation of the dynamic stall process. Bangalore and Sankar (1996) show that the formation of a leading-edge stall vortex may be inhibited by the presence of a leading-edge slat.

5. EXPERIMENTAL METHODS

So far we have discussed modeling efforts aimed at understanding and computing blade loads and the rotor wake. Experimental measurements are the foundation of helicopter design and are the main validation tool for modeling strategies. Many of the modeling results discussed so far have included experimental comparisons. In this section we examine more closely the various experimental approaches which have been used in the past, as well as those that are currently used.

The measurement of the flow field around a rotating blade is a significant challenge even at relatively low rotational speeds. For chordwise resolution and to produce the interaction of strong vortices with surfaces, rotors should have diameters of at least one meter. The facility walls must be at least one meter away from the hub. Model rotor speeds generally exceed 1000 revolutions per minute. A piece flying off such a rotor will have momentum in the plane of the rotor-disk comparable to that of a handgun bullet. Thus stress analysis, vibration diagnostics, control stations away from the tip-path plane, steel plates, and bulletproof windows are essential parts of a rotorcraft flow measurement. Rotor blades flap, teeter, pitch, bend, and twist; these motions pose problems for mechanical probes as well as in locating a point on a rotor blade in time and space to the accuracy needed for aerodynamic measurement. As shown in Figure 2, compressible flow is expected near the tip-vortex core, around the advancing blade tip, during blade-vortex interaction, and around the leading edge during dynamic stall. Elsewhere, the flowfield is generally incompressible, limiting the utility of density-gradient visualization techniques. Light-scattering techniques encounter the tradeoff between seed particle inertia and the expense of optical systems. Blade-mounted instrumentation such as sensors of surface pressure, acceleration, and shear stress must perform under extreme radial acceleration, and still have sufficient signal-to-noise ratio when transferred from the rotating to the fixed coordinate system. These considerations limit the applicability of many diagnostic advances demonstrated in fixed-wing aerodynamics and bench-scale water tunnels.

There are roughly four different sets of aerodynamic data which are sought by the helicopter aerodynamicist. These are (1) flow visualization of the rotor wake by smoke or some other nonintrusive means such as laser doppler velocimetry (LDV) or wide-field shadowgraphy; (2) direct measurement of the blade (or airframe) pressure distribution; (3) measurement of rotor inflow velocities (experimentally generated rotor inflow conditions are generally used as boundary conditions for CFD studies); and (4) direct measurement of the wake velocity field. Methods for acquisition of this data range from intrusive methods such as hot wire probes, to nominally nonintrusive means such as laser doppler velocimetry, wide-field shadowgraphy, and schleiren techniques. The flow in the rotor wake can be visualized using smoke and other seeding materials in conjunction with a laser light sheet as well. Lorber (1991) has described the use of several different visualization and measurement tools for the comprehensive description of helicopter flow fields.

In the 1950s, flight test experiments were used to validate models of the rotor wake that were based on momentum theory. Most often these measurements were done at low disk loadings and in hover or low-speed forward flight under nominally steady flow conditions. A good discussion of these time-averaged results and comparison with models based on momentum theory is given in the review of Gessow (1986).

Much of the “prescribed wake” methodology which powered classical analysis tools was developed using painstaking human analysis of photographs to accumulate vortex trajectories. Landgrebe (1972) used smoke emitted from rakes in a single plane for visualization of the wake of a two-bladed rotor. The results in Figure 15*a* show the two-dimensional cross-section of the wake. Both the tip-vortex and the inboard vortex sheet are visible on this figure. Note the significant wake contraction which had also been predicted using momentum theory. Landgrebe also demonstrated the use of conventional schleiren and laser holography.

The smoke visualizations of the rotor wake were used to develop analytical expressions for the time-averaged radial and axial positions of the helicopter wake. The axial coordinate of the tip-vortex could be accurately described by a formula of the form,

$$\begin{aligned} \bar{z} &= k_1 \psi_w \quad \text{for } 0 \leq \psi_w \leq \frac{2\pi}{b}, \\ \bar{z} &= \bar{z}_{\psi_w = \frac{2\pi}{b}} + k_2 \left(\psi_w - \frac{2\pi}{b} \right) \quad \text{for } \psi_w \geq \frac{2\pi}{b}, \end{aligned} \quad (13)$$

where \bar{z} is a nondimensional distance below the rotor disk and is normalized on the rotor radius. Here ψ_w is the azimuthal wake coordinate relative to the blade,

and b is the number of blades. k_1 and k_2 are parameters which are obtained from experiment; k_1 is found to vary linearly with $\frac{C_T}{\sigma}$ while k_2 is found to vary linearly with $\sqrt{C_T}$. The radial coordinate of the tip-vortex was found to correlate well with an equation of the form

$$\bar{r} = A + (1 - A)e^{\lambda_w \psi_w}, \quad (14)$$

where A and λ_w are constants and $A = 0.78$ and $\lambda_w = 0.145 + 27C_T$; \bar{r} is a dimensionless distance also normalized on the rotor radius. Similar wake coordinates are given for the inboard sheet. The rate of descent of an element of the tip-vortex is substantially constant prior to the passage beneath the following blade ($\psi_w \leq 60^\circ$, Figure 15*b*) at which time it jumps to another constant descent speed. These simple wake coordinate formulas are used in prescribed wake models to predict the rotor airloads. Similar formulas are discussed by Gray (1992) and a correction to these formulas for two-bladed rotors is given by Kocurek and Tangler (1976).

A major data set on which many theoretical and computational schemes are calibrated is the data set produced by Caradonna and Tung (1981). These tests involved experiments on a two-bladed untapered and untwisted planform of aspect ratio six and a NACA-0012 airfoil section. They measured blade pressure distribution and wake geometry; the pressure distribution was measured using three pressure transducers along each blade span. The wake properties were measured with a hot-wire probe oriented with the wire being tangent to the tip-path plane. Several rotor speeds were tested and the two-bladed rotor was substantially rigid.

The tip-vortex trajectory resembles the results presented by Langrebe (1972), and the tip-vortex strength was close to the maximum bound circulation on the blade sketched in Figure 5. In addition, the vortices were found to closely resemble the classical Rankine vortex structure. However, the measured blade loading and that computed using a lifting-surface with a prescribed wake do not match, leading to the conclusion by the authors that the blade spanwise loading cannot be predicted without accurate vortex location and strength.

Parthasarathy et al (1985) applied wide-field shadowgraphy to the wake of a tail rotor. This technique has the major advantages of being nonintrusive and of not requiring seeding. It uses a point source to project the path-integrated second spatial derivative of density on a retro-reflective screen. Combined with pulsed lighting and video, this technique enables quantitative analysis of the projection of vortex trajectories. Generally, depth perception is not available. Norman and Light (1987) reported measurements of the tip-vortex geometry in the wakes of two main-rotor models in hover. They observed some scatter in the data due to rotor wake instabilities as well as a short-wavelength instability

of the vortex core. They also developed an analytical model to determine the visibility of the vortex in shadowgraph images. Felker and Light (1988) extended these measurements to a 0.658-scale V-22 rotor test in hover. With the addition of a beam-splitter and a reorientation of the camera system, Bagai and Leishman (1992a) were able to significantly improve the quality of the images produced by this method.

Probe interference, nonlinearity, and sensor attrition are also alleviated using the laser velocimeter (LV), albeit at the steep price of having to use particle seeding and particle velocity as an indicator of flow velocity. An early wake study using laser Doppler velocimetry is described by Landgrebe and Johnson (1974). Desopper et al (1986) describe velocity measurements over a wide range of tip-speeds using incense seeding and a forward-scatter system whose receiving optics are rigidly coupled to the transmitting traverse by a frame around the wind tunnel test section. Liou et al (1994) measured the unsteady velocity field around a rotor blade with controlled pitch excitation of one-degree amplitude, and correlated the results with blade surface pressures and unsteady inflow prediction codes.

The circulation and structure of the tip-vortex are crucial parameters. Mba et al (1984) measured rotor blade circulation in hover by contour integration of laser velocimetry data. Thompson et al (1988) used submicron incense smoke particles to measure the flow field in the core of the tip-vortex in hover. The core axial and tangential velocity profiles at two thrust coefficients show evidence of discrete shear layers rolling up into the core. The three-dimensional compressible flow around the advancing rotor tip has been measured by Kittleson and Yu (1985). Laser schlieren visualization of the compressible flow was used with tomographic reconstruction to obtain fully three-dimensional features of the rotor wake.

McAlister et al (1995) have measured the velocity field behind a blade tip using three-color laser velocimetry and a typical result is shown in Figure 16. Note that the variation with y is typical of a vortex and that there is significant axial flow along the vortex axis (the maximum value of V_x is about $20 \frac{m}{sec}$). A similar result is presented for the inboard sheet. In addition, McAlister et al (1995) found that lowering the rotor speed does not substantially affect the general appearance of the vortex and that significant interaction between the inboard sheet and the tip-vortex is observed in the wake. A general discussion of the inability to separate the induced and form drag components in unsteady flow is also given.

The quantitative spatial and temporal precision of flow visualization is greatly enhanced using laser sheets and the video camera. Illuminated seeding patterns in thin and precisely known regions are particularly useful in quantifying

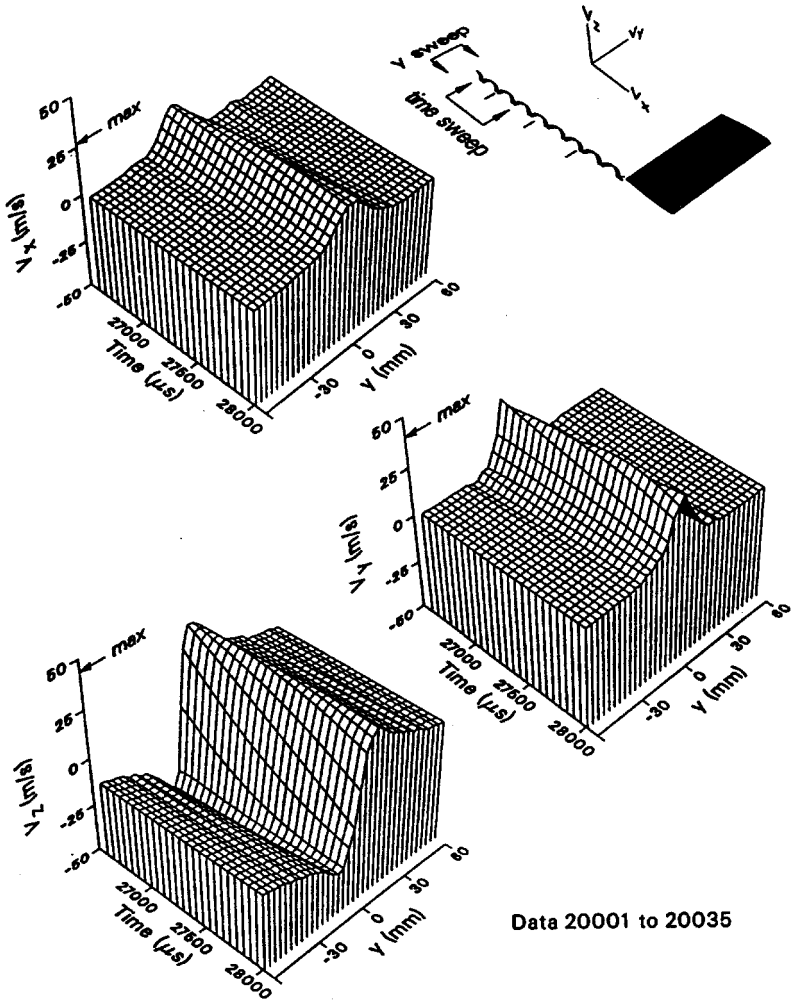


Figure 16 Velocity components along a horizontal sweep across the trailing vortex. The time frame shown corresponds to the motion of the rotor blade from 2.5 to 3.5 chord lengths past the measurement location as noted in the sketch. The rotor speed is 1100 rpm and the blade tip is at $y = 0$. From McAlister (1995).

multi-dimensional phenomena. Thompson et al (1988) constructed vortex trajectories in the near wake of a single-bladed rotor using still photographs taken from mineral oil seeding that was frozen using an argon ion laser sheet strobed with a synchronous chopper. Kim et al (1994) combined visualization using a pulsed copper vapor laser sheet and laser velocimetry to show that the edge of the inboard vortex sheet of a rigid and untwisted two-bladed rotor rolled up into a discrete structure with circulation strength approximately half that of the tip-vortex, and opposite in sign. This effect has also been observed in the video images obtained by Ghee et al (1995), but has not been investigated systematically in rotor wake models.

The first measurements of an entire planar air velocity field in rotor flows were performed by Funk et al (1993) using a double-camera system and spatial correlation velocimetry. The technique is successful in the wake, and a periodic variation was constructed from video image pairs obtained at several azimuths. However, the spatial resolution is not yet adequate to measure velocity inside the tip-vortex core. Time-averaged velocity fields have been measured using Doppler global velocimetry by Gorton et al (1995b). The technique was applied to measure time-averaged velocity near the empennage of a small-scale helicopter model, and compared to laser velocimeter data. A system of up to six cameras has been proposed to capture the three-dimensional velocity field in a light sheet. This technique has the advantage that every pixel location on the digitized image (640×480 resolutions are common now) gives one velocity vector. The disadvantages are the need for multiple cameras, the huge data reduction task involving several gigabytes of data, and the low signal-to-noise ratio at low speeds.

The rotor inflow velocity field is required for boundary conditions in both vortex method algorithms and in CFD analyses. A survey of models for non-uniform rotor inflow for use in both momentum approaches and in detailed CFD analyses of rotor wakes has been given by Chen (1990); additional experimental and computational results have been given by Elliott and Althoff (1988), Hoad et al (1988), and Hoad (1990).

6. INTERACTIONAL AERODYNAMICS

The trend in design of modern helicopters is toward more lightweight and smaller vehicles while retaining payload capability and performance parameters. This often requires that the rotor be closer to the airframe, and the higher rotor speeds required often result in higher disk loading. Thus, in recent years, one of the areas of rotorcraft aerodynamics that has received a large amount of attention is the interactional aerodynamic phenomena which occur on a helicopter. A detailed classification of a variety of aerodynamic interactions among

major components of the helicopter is given by Sheridan and Smith (1980) and these interactions are summarized in Figure 17. Two of the most important interactions are main-rotor tail-rotor interactions and wake-fuselage interactions. The intensity of these interactions depends on the relative proximity, size, shape, and flight conditions (e.g. low speed, in ground effect, flight with sideslip) of individual components.

As pointed out by McCroskey (1995), tail rotors are employed to balance the torque of the main rotor, and for better control in hover and low-speed forward flight. The performance of the tail rotor may be adversely affected if it interacts significantly with the main rotor wake. Prouty and Amer (1982) discuss the difficulties, due to poorly understood interaction effects, in designing the empennage and tail rotor. In addition, this interaction can be a significant source of noise. Additional references on this interaction are given in McCroskey (1995).

The interaction which has perhaps received the most attention is the vortex wake-fuselage interaction. This interaction process is especially intense in hover, climb, and low-speed forward flight since in these flight regimes the wake is transported almost vertically downward and may directly impinge on the surface of the fuselage. This can generate additional impulsive and periodic loading which may adversely influence the handling qualities of the aircraft and affect the fuselage loading. These loads can also be transmitted to the cabin in the form of a low-frequency vibration of the fuselage shell and thus can be annoying to passengers.

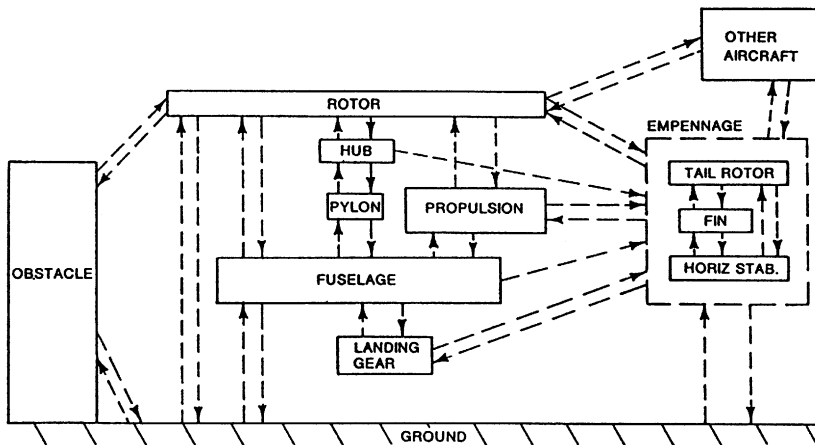


Figure 17 Summary of the many interactions among the major components of a helicopter. From Sheridan and Smith (1980).

Early work on the wake-fuselage interaction established that a smaller clearance between the rotor and the airframe will lead to higher induced airloads and vibration levels on the airframe due to the strong vortex-surface interaction (Wilson and Mineck 1975, Landgrebe et al 1977, Smith and Betzina 1986). Smith (1979) found that the presence of the fuselage distorts the wake which in turn generates enhanced blade-wake interactions; the interaction can trigger a torsional aeroelastic response by the rotor that may lead to a premature retreating blade stall.

The work described just above identified important phenomena and suggested the development of computational models of these interactions. In the mid-1980s, there were no computer codes capable of predicting even the first-order features of the time-averaged surface pressure distribution over the upper surface of the simplest fuselage geometry in hover or low-speed forward flight on the model scale. Early attempts to include airframe effects on the wake include various levels of empiricism beginning with the use of a prescribed wake structure; some of these attempts to couple the wake and the airframe are described by Crouse and Leishman (1992). Typical of these efforts is the work described by Lorber and Egolf (1990), who showed that including an unsteady potential in the rotor wake formulation improves agreement between generalized wake predictions and an experimental data set. They use the prescribed wake structure and specify the trajectory of the tip-vortex as it approaches the airframe; a fixed offset distance defines the limiting distance allowed between the tip-vortex and the airframe. The results show fair agreement with experiment; the time averaged mean pressure on the top of the airframe is in general underpredicted. Similar discrepancies appear in the instantaneous pressure on the top of the airframe. Time-averaged results for the pressure have also been obtained by Quackenbush et al (1994). The use of panel methods in the rotor-fuselage interaction problem is discussed by Dvorak et al (1977) and Clarke and Maskew (1991). The effect of the fuselage on the rotor inflow velocity field is investigated experimentally by Berry and Althoff (1990), and full-scale experiments have been conducted by Norman and Yamauchi (1991).

Liou et al (1990) trace the tip-vortex trajectory and measure the velocity near the tip-vortex as well as the pressure distribution on the surface of the airframe. Brand et al (1990) continued the work of Liou et al (1990) to show that the main features of the pressure loading of the airframe under the direct impingement of the wake are a large positive pressure load due to blade passage and an equally large suction peak due to the tip-vortex. They relate the vortex trajectory to the unsteady airframe surface pressure measured using movable microphone ports. In this way an almost continuous distribution of the airframe pressure could be

generated. They present results for the pressure on the top of the airframe at various advance ratios. The accuracy of these measurements was about 10 mm, or one core diameter; recent experiments by Peterson et al (1995) have achieved sub-millimeter accuracy using digital imaging. Leishman and Bi (1990) also report instantaneous surface pressure measurements taken at various advance ratios and note that these unsteady pressure peaks are very large and can swamp the steady mean pressure. They focus on the time history of the pressure at a fixed point on the airframe. Bagai and Leishman (1992b) found that the presence of the fuselage affects the path of the tip-vortex significantly.

Based on the work of Liou et al (1990), Brand et al (1989, 1990), and Leishman and Bi (1990), a reasonable picture of the dominant features of the unsteady pressure on the airframe under direct wake impingement conditions has emerged. For the given rotor-body separation distance, on the top of the airframe the blade passage effect generates a large positive pressure rise at $\psi = 0$ (and $\psi = \frac{2\pi}{N}$ for an N -bladed rotor), followed by a very sharp suction peak of the same order if the advance ratio is low enough so that the tip-vortex “collides” with the airframe. For a vortex whose age is $180^\circ + \psi$ (i.e. for a two-bladed rotor) at the given rotor-body separation distance of Brand et al (1990), the blade passage effect is dominant up to about $\psi = 30^\circ$ with the influence of the tip-vortex being dominant for the next $\sim 30^\circ$. Depending on the advance ratio, the maximum amplitude of the suction peak occurs near $\psi = 50^\circ$; at this time, the vortex age is 230° .

Despite the fact that the modeling efforts described so far are relatively sophisticated, all of them demonstrate limited utility in reproducing unsteady fuselage airloads. In an attempt to better understand the important features of the pressure distribution on the top of the airframe under vortex-wake collision conditions, Affes et al (1993a) use a Biot-Savart representation of the tip-vortex to calculate the tip-vortex path in the time frame from $\psi = 0^\circ$ to $\psi = 60^\circ$ for two different advance ratios. At this point in time for the two-bladed rotor studied, the vortex age is $180^\circ + \psi$. A typical result for the vortex path for $\psi > 0$ and the associated pressure, calculated from the unsteady Bernoulli equation on the top of the airframe, is depicted on Figure 18 (Affes et al 1993a). Note the good agreement with experiment; no adjustable constants are used in the analysis and only a crude model of the inboard vortex sheet is used. However, the computational results begin to deviate from the experimental results for the pressure distribution at about $\psi = 48^\circ$ and the experimental suction peak is gone by $\psi = 60^\circ$, a time scale of about 0.5 msec. The reason for this is believed to be the complete transformation of the flow in the vortex core from a high swirl velocity region characteristic of a “vortex” to a low swirl velocity region under the action of the axial velocity in the core of the vortex.

Additional experimental results (Kim and Komerath 1995) suggest that the suction peak in the pressure is convected around the retreating side of the airframe for a long period of time after it has disappeared from the top of the airframe. This effect is seen in plots of the pressure contours around the airframe from Kim and Komerath (1995) as shown in Figure 19a at a rotor phase angle of $\psi = 120^\circ$. Note that on the retreating side ($\phi < 0$; ϕ refers to the angle measured from the top of the airframe and not the zero-lift angle of attack as in Figure 1) the suction peak is still strong while on the advancing side the pressure on the airframe at a point coinciding with the vortex core is actually positive. Lee et al (1995) has demonstrated these effects for a model problem; a summary is sketched in the accompanying Figure 19b. These large-scale suction peak effects on the retreating side could be important in maneuvering

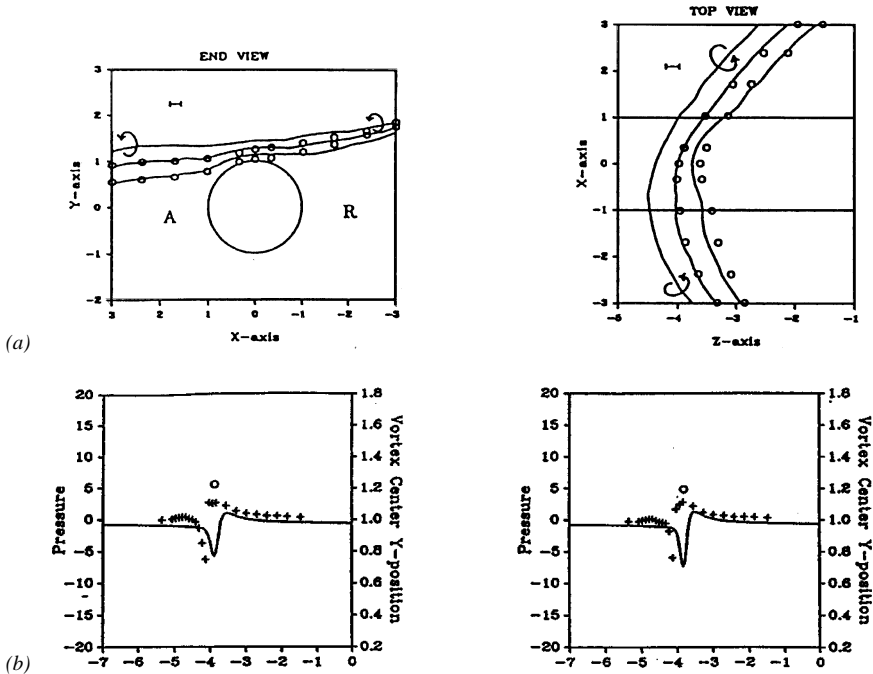
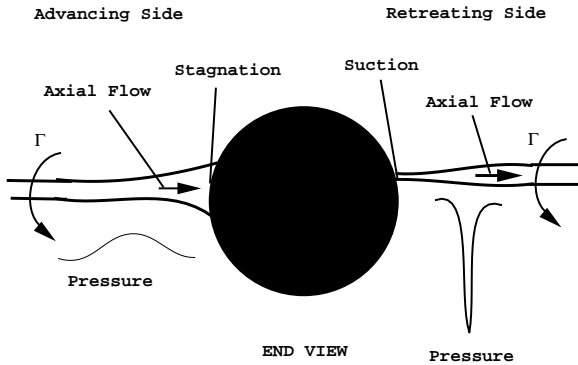


Figure 18 Comparison between computation and experiment of the vortex trajectory and pressure distribution on the top of a model airframe for advance ratio $\mu = 0.1$. The z-axis is in the direction of forward flight. (a) Tip-vortex trajectory $\psi = 0, 30, 60^\circ$; A denotes advancing side and R denotes retreating side. (b) Pressure at $\psi = 42^\circ$ on the left and $\psi = 48^\circ$ on the right. From Affes et al (1993a).



(a)



(b)

Figure 19 (a) Pressure distribution around a model airframe as measured by Kim and Komerath (1994), showing the differences exhibited on the advancing and retreating sides of the airframe. Arrows denote region below the vortex core. The angle ϕ measures distance from the top of the cylinder and $\phi > 0$ denotes the advancing blade side. $\frac{Xb}{R}$ measures distance along the airframe in the forward flight direction. (b) A sketch of the tip-vortex structure along the sides of the airframe as described by Kim and Komerath (1995) and Lee et al (1995). The vortex core radius is greatly enlarged for clarity.

flight and could be a factor in the fatigue life of the airframe. A similar effect is seen in the computations of Marshall (1994).

Steady flow Navier-Stokes simulations of the full wake-airframe interaction in forward flight have begun to be analyzed by Zori and Rajagopalan (1995). The rotor is treated as a source term in the governing equations; the magnitudes of the sources are determined from the blade geometry and aerodynamic characteristics. The detailed boundary layer behavior under the tip-vortex as it approaches the airframe is discussed by Affes et al (1993b). It is shown that flow reversal occurs in the form of an eddy which grows in time. Eventually the boundary layer fluid will wrap around the vortex fluid and this may alter its effective strength.

The sophistication of large-scale computational techniques has improved to the point that entire helicopter configurations may be incorporated. Duque and Dimanlig (1994) and Duque et al (1995) have produced results for the RAH-66 Comanche helicopter. Figure 20 depicts the streakline patterns for the V-22 Tiltrotor operating in the helicopter mode (from Meakin 1993). The V-22 is a dual purpose machine that can operate in both fixed-wing and rotary-wing modes. The computation of Meakin (1993) uses an overset grid approach in which a family of grid systems, each designed for accuracy in a particular region of the flow, are employed. Data is communicated between grids by interpolation. Overset methods are generally viewed as being more accurate



Figure 20 Streaklines for the V-22 Tiltrotor operating in the helicopter mode. From Meakin (1993).

than conventional methods at the cost of slightly higher CPU time (Bangalore and Sankar 1996).

7. SUMMARY

Modern helicopter aerodynamics is challenging because the flow field generated by a helicopter is extremely complicated and difficult to measure, model, and predict; moreover, experiments are expensive and also difficult to conduct. Helicopter aerodynamics encompasses a variety of complicated and inherently nonlinear flow phenomena including dynamic stall, blade-vortex interaction, and shock interactions. Fluid-structure interaction problems occur throughout the rotor cycle because the rotor blades undergo pitching, flapping, and aeroelastic motions dynamically in all regimes of operation. The nature of the rotor wake depends on a number of factors including the dimensions and shape of the blades, the number of blades, tip-speed, and regime of operation. Because of the complexity of the problem, current models and experiments involve a number of simplifications in order to focus on a specific aspect of the problem.

In spite of this, the past ten years have seen great advances in the understanding of isolated rotor wakes. With the advance of computational resources in recent years and the development of sophisticated experimental techniques designed to measure the fully three-dimensional character of rotor wakes, reasonable comparisons with experiment may now be obtained through computational studies at low to moderate Mach number for an isolated rotor in hover at model scale, provided aeroelastic deformations are negligible. The agreement between computations and experiment for an isolated rotor in forward flight is not as good, but advances in this regime are being made at a rapid pace. In addition, drag and moment are difficult to predict especially under stall conditions, and there is little experimental data to guide computational approaches.

At the present time, rotor design is accomplished by standard momentum theory for initial estimates of thrust and moment. These estimates are often refined using vortex methods in conjunction with lifting-line, lifting-surface, or panel methods to calculate the strength of the wake. Vortex methods are generally the least computationally demanding of the modeling approaches. CFD techniques, in the form of Navier-Stokes computations, while being substantially predictive in nature and based on first principles (apart from the specification of a turbulence model), are at the present time too computationally demanding and not accurate enough to be used extensively in design. To remedy this, methods must be sought to improve the speed and computational affordability of these programs which can only be run on a supercomputer. The use of higher-order discretization methods along with adaptive grid schemes can

reduce the computational burden and increase accuracy. It is possible that part of this improvement can be accomplished by the natural evolution of the computational hardware which is continually coming down in price and increasing in computational speed; however, it is probable that this natural evolution will not occur fast enough, and future computations will likely benefit from the use of parallel processing.

Advances in experimental techniques in the past ten years have been substantial and will continue. These advances will likely help modeling efforts. Detailed three-dimensional and unsteady measurements of the rotor wake flow are now beginning to be taken on a routine basis. However, the amount of data to be acquired and process in this activity is staggering, and efforts must be taken to process the data in a more timely and efficient manner. This process is aided by the availability of post-processing tools, normally designed for computational studies, which are now being used to reduce experimental data.

The long-range goal of any modeling effort is to be able to compute the entire unsteady flow field around a helicopter operating in any flight regime. The objective is to reduce the amount of expensive full-scale testing which is now required. However, significant barriers to this goal will exist for the foreseeable future. Rotor loads even at model scale in the forward flight and descent regimes cannot now be calculated. An additional limiting technological barrier is the issue of noise which is very acute at the higher flight speeds of modern helicopters. Noise is identified as the major impediment to increased commercial use of rotorcraft. In order to design quieter helicopters, accurate computation of BVI and high speed impulsive noise must be made; inevitably this requires a more accurate computation of the flow field itself.

The extrapolation of model-scale results to the full scale is only partially successful: Considerable differences between full-scale flight tests and full-scale wind tunnel tests are common (Tung et al 1995). At the current time, aeroelastic effects which are significant at full scale, are most often neglected in the model-scale computations.

Despite these challenges, great advances have been made in modeling the helicopter rotor wake and the flow around a helicopter during the last ten to fifteen years. Moreover, with the advances in both experimental and computational technology, progress is likely to continue at an even greater rate during the next ten years.

ACKNOWLEDGMENTS

The author is grateful to those who provided references and other information for this article. Several colleagues have made substantial contributions to the

development and organization of the paper. Dr. Thomas L. Doligalski provided a number of insights into the history and current state of rotorcraft research. Professor Narayanan Komerath wrote a substantial portion of the experimental methods section. Dr. Chee Tung provided a number of insights into the fundamentals of the problem and the prediction issues associated with modern helicopter aerodynamics. Professor Lakshmi Sankar provided valuable information on modern CFD rotor codes. A number of colleagues read at least one draft of this paper and made substantial contributions. These include Dr. Doligalski, Professor Komerath, Dr. Tung, Dr. Todd Quackenbush, and T. Alan Egolf. To these colleagues, I express my sincere thanks for their many and detailed suggestions which considerably improved the manuscript.

Visit the Annual Reviews home page at
<http://www.annurev.org>.

Literature Cited

- Affes H, Conlisk AT, Kim JM, Komerath NM. 1993a. Model for rotor tip-vortex-airframe interaction, part 2: comparison with experiment. *AIAA J.* 31(12):2274–82
- Affes H, Xiao Z, Conlisk AT, Kim JM, Komerath NM. 1993b. *The three-dimensional boundary layer flow due to a rotor tip vortex*. Presented at AIAA Fluid Dyn. Conf., 24th, Orlando.
- Ahmad J, Duque EPN. 1996. Helicopter rotor blade computation in unsteady flows using moving embedded grids. *J. Aircr.* 33:54–60.
- Bagai A, Leishman JG. 1992a. Experimental study of rotor wake/body interactions in hover. *J. Am. Hel. Soc.* 37(4):48–57.
- Bagai A, Leishman JG. 1992b. Improved wide-field shadowgraph set-up for rotor wake visualization. *J. Am. Hel. Soc.* 37(3):86–92.
- Bangalore A, Sankar LN. 1996. Forward flight analysis of slatted rotors using Navier-Stokes methods. AIAA paper 96-0675.
- Batchelor GK. 1967. *Introduction to Fluid Dynamics*. Cambridge: Cambridge Univ. Press. 615 pp.
- Beaumier P. 1994. *A coupling procedure between a rotor dynamic code and a 3D unsteady full potential code*. Presented at Am. Hel. Soc. Aeromech. Spec. Conf., San Francisco.
- Beam R, Warming RF. 1978. An implicit factored scheme for the compressible Navier-Stokes equations. *AIAA J.* 16(4):393–402.
- Berry JD, Althoff SL. 1990. *Inflow velocity perturbations due to fuselage effects in the presence of a fully interactive wake*. Presented at Annu. Forum Am. Hel. Soc., 46th, Washington D.C.
- Betz A. 1915. Die wichtigsten Grundlagen für den Entwurf von Luftschrauben. *Z. Mathematik* 6:97–103.
- Bliss DB, Teske ME, Quackenbush TR. 1987. A new methodology for free wake analysis using curved vortex elements. NASA CR 3958.
- Bliss DB, Quackenbush TR, Bilanin AJ. 1983. A new methodology for helicopter free wake analyses. *Proc. Forum Am. Hel. Soc.*, 39th.
- Bliss DB, Miller WO. 1990. Efficient free wake calculations using analytical numerical matching. *J. Am. Hel. Soc.* 38(2):43–52.
- Bliss DB, Dadone LU, Wachspress DA. 1987. Computations of rotor wake modeling for high speed applications. *Proc. Annu. Forum Am. Hel. Soc.*, 43rd.
- Bramwell ARS. 1976. *Helicopter Dynamics*. London: Edward Arnold. 408 pp.
- Brand AG, McMahan HM, Komerath NM. 1989. Surface pressure measurements on a body subject to vortex wake interaction. *AIAA J.* 27(5):569–74.
- Brand AG, McMahan HM, Komerath NM. 1990. Correlations of rotor wake airframe interaction measurements and flow visualization data. *J. Am. Hel. Soc.* 35(4):4–15.
- Brand AG. 1989. *An experimental investigation of the interaction between a model rotor and airframe in forward flight*. PhD thesis. Georgia Inst. Technol.
- Bridgeman JO, Steger JL, Caradonna FX. 1982. A conservative finite-difference algorithm for

- the unsteady transonic potential equation in generalized coordinates. AIAA paper 82-1388.
- Caradonna FX. 1992. The application of CFD to rotary wing aircraft. NASA TM 102803.
- Caradonna FX, Tung C. 1981. Experimental and analytical studies of a model helicopter rotor in hover. NASA TM 81232.
- Caradonna FX, Strawn RC, Bridgeman JO. 1988. An experimental and computational study of rotor-vortex interactions. *Proc. Eur. Rotorcraft Forum, 14th, Milano*.
- Carr LW. 1988. Progress in analysis and prediction of dynamic stall. *J. Aircr.* 25(1):6-17.
- Carr LW, Chandrasekhara MS. 1995. *An assessment of the impact of compressibility on dynamic stall*. AIAA paper 95-0779. Presented at Aerosp. Sci., 33rd, Reno, Nevada.
- Castles W, Gray RB. 1951. Empirical relation between induced velocity, thrust, and rate of descent of a helicopter rotor as determined by wind tunnel tests on four model rotors. NACA TN-2474.
- Chang I-C, Tung C. 1985. Numerical solution of the full-potential equation for rotors and oblique wings using a new wake model. AIAA paper 85-0268.
- Chen RTN. 1990. A survey of nonuniform inflow models for rotorcraft flight dynamics and control applications. *Vertica* 14:147-90.
- Crouse GL, Leishman JG. 1992. *Interactional aerodynamic effects on rotor performance in hover and forward flight*. Presented at Annu. Forum Am. Hel. Soc., 48th, Washington D.C.
- Crouse GL, Leishman JG. 1993. A new method for improved free-wake convergence in hover and low-speed forward flight. Presented at Aerosp. Sci. Meet., 21st.
- Desopper A, Lafon P, Ceroni P, Phillippe JJ. 1986. Ten years of rotor flow studies at ONERA: state of the art and future studies. *Proc. Annu. Forum Am. Hel. Soc.*, 42nd, Washington, D.C.
- Duque EPN, Dimanlig ACB. 1994. *Navier-Stokes simulation of the AH-66 (Comanche) helicopter*. Presented at Am. Hel. Soc. Aeromech. Spec. Conf., San Francisco.
- Duque EPN, Berry JD, Dimanlig ACB, Budge AM. 1995. *A comparison of computed and experimental flowfields of the RAH-66 helicopter*. Presented at Am. Hel. Soc. Spec. Meet. on Aeromech. Tech. Prod. Des., Bridgeport, Conn.
- Duque EPN, Biswas R, Strawn RC. 1995. *A solution adaptive structured/unstructured overset grid solver with applications to helicopter rotor flows*. AIAA paper 95-1766. Presented at Appl. Aerodyn. Conf., 13th, San Diego, Calif.
- Dvorak FA, Maskew B, Woodward FA. 1977. USAAMRDL Tech. Rep. 77-4, Eustis Directorate, U.S. Army Air Mobility Research and Development Laboratory, Fort Eustis, VA.
- Egolf TA. 1988. *Helicopter free-wake prediction of complex wake structures under blade-vortex interaction operating conditions*. *Proc. Annu. Forum Am. Hel. Soc.*, 44th, Washington DC, pp. 819-32.
- Egolf TA, Landgrebe AJ. 1983. Helicopter rotor wake geometry and its influence in forward flight. Vol. 1: Generalized wake geometry and wake effect on rotor airloads and performance. NASA CR 3726.
- Egolf TA, Sparks SP. 1986. A full potential rotor analysis with wake influence using an inner-outer domain technique. *Proc. Annu. Forum Am. Hel. Soc.*, 42nd, pp. 997-1011.
- Elliott JW, Althoff SL. 1988. Inflow measurement made with a laser velocimeter on a helicopter model in forward flight. Volumes. I-V, NASA TM 100541-100545
- Felker FF, Light JS. 1988. Aerodynamic interactions between a rotor and wing in hover. *J. Am. Hel. Soc.* 33(2):53-61.
- Funk R, Fawcett PA, Komerath NM. 1993. Instantaneous velocity fields in a rotor wake by spatial correlation velocimetry. AIAA Paper 93-3081, Fl. Dyn. Conf., 24th, Orlando, Fla.
- Gallman JM et al. 1995. *Effect of wake structure on blade-vortex interaction phenomena: acoustic prediction and validation*. Presented at CEAS/AIAA Aeroacoustic Conf., 1st, Munich.
- Gennaretti M, Morino L. 1992. A boundary element method for the potential, compressible aerodynamics of bodies in arbitrary. *Aero. J. Roy. Aero. Soc.*
- Gessow A. 1986. Understanding and predicting helicopter behavior—then and now. *J. Am. Hel. Soc.* 31(1):3-28.
- Gessow A, Myers G. 1952. *Aerodynamics of Helicopter*. New York: Frederick Ungar
- Ghee T, Berry JD, Zori LAJ, Elliott JW. 1995. Wake geometry measurements and analytical calculations on a small-scale rotor model. NASA TP 3584.
- Glauert H. 1922. An aerodynamic theory of the airscrew. *British ARC R & M* 786.
- Glauert H. 1928. On horizontal flight of a helicopter. *R & M* 1157.
- Gorton SA, Poling DR, Dadone L. 1995a. Laser velocimetry and blade pressure measurements of a blade-vortex interaction. *J. Am. Hel. Soc.* 40(2):15-23.
- Gorton S, Meyers J, Berry JD. 1995b. Velocity measurements near the empennage of a small-scale helicopter model. *Proc. Annu. Forum Am. Hel. Soc.*, 51st.
- Gray RB. 1955. On the motion of the helical vortex shed from a single-bladed hovering helicopter rotor and its application to the cal-

- ulation of the spanwise aerodynamic loading. Princeton Univ. Aero. Engr. Dept., Report 313.
- Gray RB. 1956. An aerodynamic analysis of a single-bladed rotor in hovering and low-speed forward flight as determined from smoke studies of the vorticity distribution in the wake. Princeton Univ. Aero. Engr. Dept., Report 356.
- Gray RB. 1992. Vortex modelling for rotor aerodynamics—the 1991 Alexander A. Nikolsky Lecture. *J. Am. Hel. Soc.* 37(1):3–14.
- Ham ND, Garelick MS. 1968. Dynamic stall considerations in helicopter rotors. *J. Am. Hel. Soc.* 13(2):49–55.
- Hardin JC, Lamkin SL 1986. An Euler code calculation of blade-vortex interaction noise. Winter Annual Meeting of the American Society of Mechanical Engineers. Paper 86-WANCA-3.
- Hassan AA, Tung C, Sankar, LN. 1992. Euler solutions for self-generated rotor blade-vortex interactions. *Int. J. Num. Meth. Fluids.* 15:427–51.
- Heller H, Schultz K-J, Ahmed SR. 1994. Unsteady surface pressure characteristics on helicopter blades: a key to the physics of rotor noise. 19th ICAS Congress, paper 94-2.7.2, Anaheim, CA.
- Hess JL, Smith AMO. 1972. Calculation of potential flow about arbitrary bodies. In *Progress in the Aeronautical Sciences*, Vol. 8. New York: Pergamon.
- Hess JL. 1990. Panel methods in computational fluid dynamics. *Annu. Rev. Fluid Dynamics.*
- Hoad DR. 1990. Rotor induced-inflow-ratio measurements and CAMRAD calculations. NASA TP 2946, January 1990.
- Hoad DR, Althoff SL, Elliott JW. 1988. Rotor inflow variability with advance ratio. Proceedings of the 44th Annual Forum of the Am. Hel. Soc., Washington DC, June 16-18, 1988, pp. 57–72.
- Jameson A, Caughey DA. 1977. Numerical calculation of the transonic flow past a swept wing. ERDA Research and Development, Mathematics and Computing, June 1977.
- Johnson W. 1971. A lifting-surface solution for vortex-induced airloads. *AIAA J.* 9(4):689–695.
- Johnson W. 1980. *Helicopter Theory*. Princeton, NJ: Princeton Univ. Press.
- Johnson W. 1986. Recent developments in rotary-wing aerodynamic theory. *AIAA J.* 24(8):1219–44.
- Katz J, Plotkin A. 1991. *Low-Speed Aerodynamics from Wing Theory to Panel Methods*. New York: McGraw Hill.
- Kim JM, Komerath NM. 1995. Summary of the interaction of a rotor wake with a circular cylinder. *AIAA J.* 33(3):470–8.
- Kim JM, Komerath NM, Liou SG. 1994. Vorticity concentration at the edge of the inboard vortex sheet. *J. Am. Hel. Soc.* 39(2):30–4.
- Kittleston JK, Yu Y. 1985. Transonic rotor flow measurement technique using holographic interferometry. *J. Am. Hel. Soc.* 30(4):3–10.
- Klemin A. 1945. Principles of rotary-wing aircraft. AERO Digest, May 1 and June 1, 1945.
- Kocurek JD, Tangler JL. 1976. A prescribed wake lifting surface hover performance analysis. Proceedings of the 32nd Forum of the Am. Hel. Soc., May. Preprint 1001.
- Landgrebe AJ. 1972. The wake geometry of a hovering rotor and its influence on rotor performance. *J. Am. Hel. Soc.* 17(4):3–15.
- Landgrebe AJ, Johnson BV. 1974. Measurements of model helicopter rotor flow velocities with a laser Doppler velocimeter. *J. Am. Hel. Soc.* 19(3):39–43.
- Landgrebe AJ. 1994. New directions in rotorcraft computational aerodynamics research in the U. S. 75th AGARD Fluid Dynamics Panel Meeting on Aerodynamics and Aeroacoustics of Rotorcraft, Berlin.
- Landgrebe AJ, Moffitt RC, Clark DR. 1977. Aerodynamic technology for advanced rotorcraft. *J. Am. Hel. Soc.* 22 (2, 3)
- Lee J, Xiao Z, Burggraf OR, Conlisk AT, Komerath NM. 1995. An inviscid analysis of vortex-surface collisions. AIAA paper 95-2237.
- Leishman JG, Bi N. 1990. Aerodynamic interactions between a rotor and a fuselage in forward flight. *J. Am. Hel. Soc.* 35(3):22–31.
- Leishman JG, Baker A, Coyne A. 1995. Measurements of rotor tip vortices using three-component laser Doppler velocimetry. Am. Hel. Soc. Specialists' Meeting on Aeromechanics Technology and Product Design, Bridgeport, Conn.
- Leishman JG, Beddoes TS. 1989. A semi-empirical model for dynamic stall. *J. Am. Hel. Soc.* 34(3):3–17.
- Liou SG, Komerath NM, McMahon HM. 1989. Velocity measurements of airframe effects on a rotor in low-speed forward flight. *J. Aircraft* 26(4):340–8.
- Liou SG, Komerath NM, Lal MK. 1994. Measurement around a rotor blade excited in pitch. Part 1: Dynamic inflow. *J. Am. Hel. Soc.* 39(2):3–12.
- Liou SG, Komerath NM, McMahon HM. 1990. Measurement of the interaction between a rotor tip-vortex and a cylinder, *AIAA J.* 28(6):975–981.
- Lock 1924. Experiments to verify the independence of the elements of an airscrew blade. British R & M 853.
- Loewy, RG. 1957. A two-dimensional approximation to the unsteady aerodynamics of rotary wings. *J. Aero. Sci.* 24(2):81–92.

- Lorber PF, Egoft TA. 1990. An unsteady rotor-fuselage interaction analysis. *J. Am. Hel. Soc.* 35(7):32-42.
- Lorber PF. 1991. Aerodynamic results of a pressure-instrumented model rotor test at the DNW. *J. Am. Hel. Soc.*, 36(4):66-76.
- Lorber PF. 1993. Tip vortex, stall vortex, and separation observations on pitching three-dimensional wings. AIAA 24th Fluid Dynamics Conference, Orlando, Fla.
- Lorber PF, Carta FO. 1988. Airfoil dynamic stall at constant pitch rate and high Reynolds number. *J. Aircraft* 25(6):548-556.
- Lorber PF, Stauter RC, Haas RJ, Anderson TJ, Torok MS, Kohlhepp FW. 1994. Techniques for comprehensive measurement of model helicopter rotor aerodynamics. Proceedings of the 50th Forum of the Am. Hel. Soc., May 11-14, 1994, pp. 797-814.
- Mangler KW, Squire HB. 1950. The induced velocity field of a rotor. R & M 2642.
- Maskew B. 1986. VSAERO theory document. NASA CR-4023, November, 1986.
- Marshall JS. 1994. Vortex cutting by a blade. Part II: Computations of vortex response. *AIAA J.* 32(7):1428-36.
- Mba MN, Meylan C, Mansca C, Favier D. 1984. Radial distribution of circulation of a rotor in hover measured by a laser velocimeter. Proceedings of the Tenth European Rotorcraft Forum, The Hague, Netherlands.
- McAlister KW, Schuler CA, Branum L, Wu JC. 1995. 3-D measurements near a hovering rotor for determining profile and induced drag. NASA TP 3577, August 1995.
- McCormick BW. 1967. *Aerodynamics of VSTOL Flight*. New York:Academic Press.
- McCroskey WJ. 1995. Vortex wakes of rotorcraft. AIAA paper 95-0530.
- McCroskey WJ. 1981. The phenomenon of dynamic stall. NASA TM 81264, March.
- Meakin RL. 1993. Moving body overset grid methods for complete tiltrotor simulations, AIAA paper 93-3350-CP. Presented at the 11th AIAA Computational Fluid Dynamics Conference, Orlando, FL, July 1993.
- Miller WO. 1993. A fast adaptive resolution method for efficient free wake calculations. Proceedings of the 49th Forum of the Am. Hel. Soc., May 19-21, 1993, pp. 617-30.
- Miller WO, Bliss DB. 1993. Direct periodic solutions of rotor free wake calculations. *J. Am. Hel. Soc.* 38(2):53-60. First presented at the Proceedings of the 46th Forum of the Am. Hel. Soc., 1990.
- Moore DW. 1972. Finite amplitude waves on aircraft trailing vortices. *Aero. Quart.* 23:307-14.
- Morino L, Kaprielian Z, Sipcic SR. 1985. Free wake analysis of helicopter rotors. *J. Aircraft* 9(2):127-40.
- Morino L, Gennaretti M. 1991. Boundary integral equation methods for aerodynamics. In *Computational Nonlinear Mechanics in Aerospace Engineering*, ed. S. N. Atluri. Prog. Astronaut. Aeronaut. 147:
- Norman TR, Light JS. 1987. Rotor tip-vortex geometry measurements using the wide-field shadowgraph technique. *J. Am. Hel. Soc.* 32(2):40-50.
- Norman TR, Yamauchi GK. 1991. Full-scale investigation of aerodynamic interactions between a rotor and a fuselage. Proceedings of the 47th Annual Forum of the Am. Hel. Soc., pp. 461-86.
- Parthasarathy SP, Cho YI, Black LH. 1985. Wide-field shadowgraph flow visualization of tip vortices generated by a helicopter rotor. AIAA 85-1557, July 1985.
- Peterson K, Frank RB, Mahalingam R, Komerath NK, Conlisk AT. 1995. Recent experiments on vortex collision with a cylinder. AIAA 95-2236.
- Phillipe JJ, Roesch P, Dequin AM, Cler A. 1985. A survey of recent developments in helicopter aerodynamics. AGARD-LS-139. *Helicopter Aeromechanics*, April 1985, pp. 2-1-2-40.
- Prouty RW, Amer KB. 1982. The YAH-64 empennage and tail rotor—a technical history. Proceedings of the 38th Annual Forum of the Am. Hel. Soc., May 4-7, 1982, pp. 247-61.
- Quackenbush TR, Bliss DB, Wachpress, DA. 1989. Free wake analysis of rotor configurations for reduced vibratory airloads. Proceedings of the AHS National Specialists' Meeting on Rotorcraft Dynamics, November.
- Quackenbush TR, Lam C-MG, Bliss DB. 1994. Vortex methods for the computational analysis of rotor/body interaction. *J. Am. Hel. Soc.* 39(4):14-24.
- Ramachandran K, Schlechtriem S, Caradonna FX, Steinhoff, J. 1993. The application of vorticity embedding to the computation of advancing rotor flows. Presented at Annu. Forum Am. Hel. Soc., 49th, May 19-21, 1993, pp. 571-84.
- Ramachandran K, Tung C, Caradonna FX. 1989. Rotor hover performance prediction using a free-wake, computational fluid dynamics method. *J. Aircraft* 26:1105-10.
- Rankine, WJ. 1865. On the mechanical principles of the action of ship propellers. *Trans. Inst. Naval Arch.* 6:13-39.
- Reichert G. 1985. Helicopter aeromechanics—introduction and historical review. AGARD-LS-139. *Helicopter Aeromechanics*, April 1985, pp. 1-1-1-23.
- Sarpkaya, T. 1989. Computational methods with vortices. The 1988 Freeman Scholar lecture. *J. Fluids Engineering* 111:5-52.
- Scully MP. 1967. A method of computing helicopter rotor wake distortion. Massachusetts

- Institute of Technology, ASRL TR 138-1, June.
- Seddon J. 1990. *Basic Helicopter Aerodynamics*. BSP Professional Books.
- Sheridan PF, Smith RF. 1980. Interactional aerodynamics—a new challenge to helicopter technology. *J. Am. Hel. Soc.* 25(1):3–21.
- Shivananda TP, McMahon HM, Gray RB. 1978. Surface pressure measurements at the tip of a model helicopter rotor in hover. *J. Aircraft* 15:460–7.
- Shultz LA, Panda B, Tarzanin, FJ, Derham RC, Oh BK, Dadone L. 1994. Interdisciplinary analysis for advanced rotors—approach, capabilities, and status. Presented at Am. Hel. Soc. Aeromech. Spec. Conf., San Francisco, Calif, January 19–21.
- Smith CA. 1979. Some effects of wake distortion due to fuselage flow field on rotor thrust limits. Army Research Office Workshop on Rotor Wake Technology, Raleigh, NC, April 1979.
- Smith CA, Betzina MD. 1986. Aerodynamic loads induced by a rotor on a body of revolution. *J. Am. Hel. Soc.* 31 no 1:4–15.
- Srinivasan, GR, McCroskey, WJ 1988a. Navier-Stokes calculations of hovering rotor flowfields. *J. Aircraft* 25(10):865–74.
- Srinivasan GR, McCroskey WJ. 1988b. Unsteady interaction of a rotor with a vortex. AIAA paper 89-1848.
- Srinivasan GR, Raghavan V, Duque EPN, McCroskey, WJ. 1993. Flowfield analysis of modern helicopter rotors in hover by Navier-Stokes method. *J. Am. Hel. Soc.* 38(3):3–13.
- Srinivasan GR, Ekaterinaris JA, McCroskey WJ. 1995. Evaluation of turbulence models for unsteady flows of an oscillating airfoil. *Computers and Fluids* 24(7):833–61.
- Srinivasan GR, Baeder JD, Obayashi S, McCroskey WJ. 1992. Flowfield of a lifting rotor in hover: a Navier-Stokes simulation. *AIAA J.* 30(10):2371–2378.
- Srinivasan GR, Baeder JD. 1993. TURNS: A free-wake Euler-Navier-Stokes numerical method for helicopter rotors. *AIAA J.* 31(5):959–962.
- Srinivasan GR, Sankar LN. 1995. Status of Euler and Navier-Stokes CFD methods for helicopter applications. Presented at the Am. Hel. Soc. Specialists' Meeting on Aeromechanics Technology and Product Design, Bridgeport CT, October 11–13, 1995.
- Steinhoff J, Ramachandran K. 1990. Free wake analysis of compressible rotor flows. *AIAA J.* 28(3):426–431. See also *Vertica* 13(2):133 (1989).
- Steinhoff J, Suryanarayanan K. 1983. The treatment of vortex sheets in compressible potential flow. AIAA paper 83-1881.
- Steinhoff J, Raviprakash GK. 1995. Navier-Stokes computation of blade-vortex interaction using vorticity confinement. AIAA paper 95-0161.
- Steinhoff J. 1994. Vorticity confinement: a new technique for computing vortex dominated flows. In *Frontiers of Computational Fluid Dynamics*, ed. DA Caughey, MM Hafez. Chichester: Wiley
- Stepniewski WZ, Keys CN 1984. *Rotary-Wing Aerodynamics*, Vols 1 and 2. New York: Dover Publications
- Strawn RC. 1991. Wing-tip-vortex calculations with an unstructured adaptive-grid Euler solver. Proceedings of the 47th Annual Forum of the Am. Hel. Soc., Alexandria VA, pp. 65–76.
- Strawn RC, Barth TJ. 1993. A finite-volume Euler solver for computing rotary-wing aerodynamics on unstructured meshes, *J. Am. Hel. Soc.* 38(2):61–7.
- Strawn RC, Caradonna FX. 1987. Conservative full potential method for unsteady transonic rotor flows. *AIAA J.* 25(2):193–8.
- Summa, JM. 1976. Potential flow about impulsively started rotors, *J. Aircraft* 13(4):317–9.
- Summa JM, Clark DR 1979. A lifting-surface method for hover climb airloads. Presented at the 35th Annual Forum of Am. Hel. Soc., Washington D.C.
- Thompson TL, Komerath NM, Gray RB. 1988. Visualization and measurement of the tip-vortex core of a rotor blade in hover. *J. Aircraft* 25(12):1113–21.
- Torok MS, Berezin CR. 1993. Aerodynamic and wake methodology evaluation using model UH-60A experimental data. *J. Am. Hel. Soc.* 39(2):21–9.
- Tung C, Lee S. 1994. Evaluation of hover prediction codes. Proceedings of the 50th Annual Forum of the Am. Hel. Soc., Washington, DC, May 11–13, 1994, pp. 829–44.
- Tung C, Bousman WG, Low S. 1995. A comparison of airload data between model-scale rotor and full-scale flight test. Am. Hel. Soc. Specialists' Meeting on Aeromechanics Technology and Product Design, Bridgeport CT, October 11–13, 1995.
- Wake BE, Lorber PF. 1993. Dynamic stall correlation of a rotorwing Navier-Stokes solver on a massively parallel computer. Presented at the 50th Annual Forum of the Am. Hel. Soc., St Louis, May 19–21.
- Wake BE, Sankar LN. 1989. Solutions of the Navier-Stokes equations for the flow about a rotor blade. *J. Am. Hel. Soc.* 34 no 2:13–23. First presented at the National Specialists, Meeting on Aerodynamics and Aeroacoustics, Feb. 25–27, 1987, Arlington, TX.
- Wake BE, Egolf TA. 1990. Implementation of a rotary-wing Navier-Stokes solver on a mas-

- sively parallel computer. *AIAA J.* 29(1):58–67.
- Wilson JC, Mineck RE. 1975. Wind-tunnel investigation of helicopter rotor wake effects on three helicopter fuselage models. NASA TM X-3185, March 1975.
- Yu YH. 1995. Rotor blade vortex interaction noise: generating mechanisms and its control concepts. Am. Hel. Soc. Specialists' Meeting on Aeromechanics Technology and Product Design, Bridgeport CT, October 11–13, 1995.
- Yu YH, Lee S, McAlister KW, Tung C, Wang CM. 1995. Dynamic stall control for advanced rotorcraft application. *AIAA J.* 33(2):289–95.
- Zori LAJ, Rajagopalan RG. 1995. Navier-Stokes calculations of rotor-airframe interaction in forward flight. *J. Am. Hel. Soc.* 40(2):57–67.